SCHOOL OF
CIVIL ENGINEERING

INDIANA
DEPARTMENT OF HIGHWAYS

JOINT HIGHWAY RESEARCH PROJECT

FHWA/IN/JHRP-88/3 -1

Final Report

AN AUTOMATIC, QUANTITATIVE IMAGE ANALYSIS SYSTEM FOR CONSTRUCTION MATERIALS

Dexiang Shi

PURDUE UNIVERSITY

JOINT HIGHWAY RESEARCH PROJECT

FHWA/IN/JHRP-88/3

Final Report

AN AUTOMATIC, QUANTITATIVE IMAGE ANALYSIS SYSTEM FOR CONSTRUCTION MATERIALS

Dexiang Shi

AN AUTOMATIC, QUANTITATIVE IMAGE ANALYSIS SYSTEM
FOR CONSTRUCTION MATERIALS

Final Report

TO: H. L. Michael, Director
Joint Highway Research Project

January 26, 1988

Project: C-36-58C

FROM: D. N. Winslow, Research Engineer
Joint Highway Research Project

File: 5-12-3

Attached is the Final Report on the HPR Part II study titled "Image Analysis of Highway Materials." The report was written by Dexiang Shi, Graduate Research Assistant, under my direction. The report discusses the development of an automatic quantitative image analysis (AQIA) software system specially designed for materials' analysis. It is implemented on a UNIX operating system with a Tektronix graphics terminal, as was specified in the study proposal.

The report is forwarded to IDOH and FHWA in fulfillment of the objectives of the study.

Sincerely yours,

D. N. Winslow
Research Engineer

DNW/mlc

cc: A.G. Altschaeffl
J.M. Bell
M.E. Cantrall
W.F. Chen
W.L. Dolch
R.L. Eskew
J.D. Fricker
D.E. Hancher
R.A. Howden
M.K. Hunter
J.P. Isenbarger
J.F. McLaughlin
K.M. Mellinger
R.D. Miles
P.L. Owens
B.K. Partridge
G.T. Satterly
C.F. Scholer
K.C. Sinha
C.A. Venable
T.D. White
L.E. Wood

AN AUTOMATIC, QUANTITATIVE IMAGE ANALYSIS SYSTEM FOR CONSTRUCTION MATERIALS

by

Dexiang Shi
Graduate Research Assistant

Joint Highway Research Project

Project No.: C-36-58C

File No.: 5-12-3

Prepared as Part of an Investigation

Conducted by

Joint Highway Research Project
Engineering Experiment Station
Purdue University

in cooperation with the

Indiana Department of Highways

and the

U.S. Department of Transportation
Federal Highway Administration

Purdue University
West Lafayette, Indiana

January 26, 1988

TECHNICAL REPORT STANDARD TITLE PAGE

1. Report No.	2. Government Accession No.	3. Recipient's Catalog No.
FHWA/IN/JHRP-88/3		

4. Title and Subtitle
An Automatic, Quantitative Image Analysis System for Construction Materials

5. Report Date
26 January 1988

6. Performing Organization Code

7. Author(s)
Shi, Dexiang

8. Performing Organization Report No.
JHRP-88/3

9. Performing Organization Name and Address
Joint Highway Research Project
Civil Engineering Building
Purdue University
West LaFayette, Indiana - 47907

10. Work Unit No.

11. Contract or Grant No.
HPR Part II

12. Sponsoring Agency Name and Address
Indiana Department of Highways
State Office Building
100 North Senate Avenue
Indianapolis, Indiana - 46204

13. Type of Report and Period Covered
Final Report

14. Sponsoring Agency Code

15. Supplementary Notes
Conducted in cooperation with the U.S. Department of Transportation, Federal Highway Administration.

16. Abstract

An image analysis software system has been developed for a UNIX operating system and a Tektronix terminal. It is designed for the particles and/or pores in construction materials. This system provides a means to measure many discrete fields of view, in order to obtain statistically meaningful results. The system can process images from either an electron or light microscope, or from an ordinary camera. Either negatives or positives can be used. A new method based on fuzzy probability has been developed to segment digital images into binary images. It is more consistent than existing techniques. The accuracy of the system has been verified with images having known geometric properties. Measurements have an error of less than 1% with an image of appropriate resolution. The system makes different measurements on separate particles and cut planes through massive samples. In the former case, the measurements are: the perimeters, areas, and maximum chords of particles in orthogonal directions, the maximum, minimum and mean values of these parameters, and their distributions. Also, the area of the image, the area faction of particles and the number of particles are measured. In the case of the cut planes, the estimated parameters are: volume fraction of particles, surface area per unit bulk volume, and surface area per unit particle volume. The size distribution, total number of particles and mean diameter can also be estimated.

17. Key Words	18. Distribution Statement
Image Analysis, Construction Materials, Fuzzy Sets, Fuzzy Probability Thresholding	No restrictions. This document is available to the public through the National Technical Information Service, Springfield, Virginia 22161.

19. Security Classif. (of this report)	20. Security Classif. (of this page)	21. No. of Pages	22. Price
Unclassified	Unclassified	129	

Form DOT F 1700.7 (8-69)

ACKNOWLEDGEMENTS

The author would like to express his appreciation for the continual encouragement and guidance of his major professor, Dr. Douglas N. Winslow, without which this research would have not been possible.

Thanks are also due to the other members of the advisory committee, Dr. James T. P. Yao, Dr. W. L. Dolch and Dr. Terry R. West, for their assistance.

This investigation was supported by the Indiana Department of Highway and the Federal Highway Administration through the Joint Highway Research Project at Purdue.

TABLE OF CONTENT

Page

LIST OF TABLES

LIST OF FIGURES

ABSTRACT

Shi,Dexiang. Ph.D, Purdue University, December, 1987. An automatic quantitative image analysis system for construction materials. Major Professor: Douglas N. Winslow.

An image analysis software system has been developed for a UNIX operating system and a Tektronix terminal. It is designed for the particles and/or pores in construction materials. This system provides a means to measure many discrete fields of view, in order to obtain statistically meaningful results.

The system can process images from either an electron or light microscope, or from an ordinary camera. Either negatives or positives can be used. A new method based on fuzzy probability has been developed to segment digital images into binary images. It is more consistent than existing techniques.

The system uses object labeling. This makes spot filling, noise filtering, separation of touching objects, object counting and measurement of individual objects easier.

The accuracy of the system has been verified with images having known geometric properties. Measurements have an error of less than 1% with an image of appropriate resolution.

The system makes different measurements on separate particles and cut planes through massive samples. In the former case, the measurements are: the perimeters, areas, and maximum chords of particles in orthogonal directions, the maximum, minimum and mean values of these parameters, and their distributions. Also, the area of the image, the area faction of particles and the number of particles are measured.

In the case of the cut planes, the estimated parameters are: volume fraction of particles, surface area per unit bulk volume, and surface area per unit particle volume. The size distribution, total number of particles and mean diameter can also be estimated.

A new method based on computer simulation has been developed to estimate size distribution of particles of any modelable shape. Older methods have a tendency to give too large a number of small particles, and the new method does not.

INTRODUCTION

The goal of quantitative microscopy is to measure the geometric properties of particles or microstructures. In the cement and concrete area, for example, the measurement of particles may be to determine the size distribution of flyash or fine aggregate. The measurement of microstructures may be to determine the air content in concrete, the size distribution of pores in cement or concrete, the phase distribution in cement, etc. These examinations are performed on two dimensional images. Stereology is used to estimate statistically the three dimensional properties from the direct measurements made on the two dimensional images [1,2].

Optical and electron microscopic examinations have been used for years in quantitative microscopy. Such a manual examination is a time consuming and tedious process. In order to obtain statistically meaningful results, it is usually required that many measurements be made. This requirement has been ignored sometimes because of the effort that would be required.

Recently, the computer image analysis technique has been applied to quantitative microscopy [3-11]. In general, computer image analysis can be quantitative or non-quantitative. A robot vision system is a typical application of non-quantitative image analysis. Its major objective is to recognize objects, or match objects to models. Quantitative microscopy is a typical application of quantitative image analysis. Its objective is to measure the sizes of the objects of interest. Because the major advantage of a computer is its capability of processing data, computer image analysis makes practical the measurement of many objects in many images. Therefore, the statistical requirements can be satisfied with little human effort.

The process of quantitative image analysis is as follows. The original, analog image is first transformed into a digital image by a digitizer. A digital image is a two dimensional array of numbers, each number representing the light intensity, or gray level, of the corresponding point in the original image [12]. The points are usually called pixels. In order to display the image on a monitor, the digital image must be segmented into a binary image for monochromatic monitors, or a multiplex image for polychromatic monitors. A binary image consists of two types of pixels: object pixels and background pixels. A multiplex image may have more than one type of object

pixel, each with a differing gray level. Finally, the desired geometric properties of the objects of interest are measured by the computer on the segmented image.

These steps in the process are roughly paralleled in the organization of the chapters that follow. First there is a chapter on the unique statistical situation involved in the combined analysis of multiple images of the same material. It allows the user to assign an accuracy to a given measurement. The next section describes several available methods of segmenting an image into object and background in preparation for measurements. It includes a unique user-independent method based on fuzzy set theory. This is followed by a chapter on procedures that can be invoked to improve faulty, previously segmented images so that subsequent measurements will be more accurate. These procedures allow the user to "edit" an image based on his/her knowledge of the displayed objects. Finally, there is a chapter describing the basis for the various measurements that can be performed on the segmented and, if necessary, improved image. It includes a unique method for size distribution estimation by using computer simulation. This is followed by a chapter that demonstrates some typical results that a user might get when analyzing a variety of images. Lastly, a chapter is included that is a guide to the use of the various programs that make up this unique analysis package.

Some images are of discrete particles. In this case, one can view the full profile of each particles. When this is the case, the following measurements can be made on the image.

1. Total number of particles
2. Number of particles per unit image area
3. Projected perimeters of particles
4. Projected areas of particles
5. Projected maximum chords of particles
6. Distribution of projected perimeters
7. Distribution of projected areas
8. Distribution of projected maximum chords
9. Maximal, minimal and mean values of projected perimeters
10. Maximal, minimal and mean values of projected areas
11. Maximal, minimal and mean values of projected maximum chords

Other images are of a plane cut through a solid mass of some material. Such a plane will generally intersect imbedded objects that are of interest. The following parameters can be determined from measurements of these intersected objects.

1. Volume fraction of objects
2. Surface area of objects per unit bulk volume
3. Specific surface area of objects per unit object volume
4. Size distribution of objects
5. Number of objects per unit bulk volume

6. Mean size of objects

7. Mean value of the maximum dimensions of objects

Computer image analysis has another advantage over manual examination. The volume fraction of a phase can be estimated from the area fraction of a cut plane, using areal analysis, or lineal traverse, or point counting (random or systematic) [13]. For manual examinations, only lineal traverse and point counting are practical possibilities. But, it has been proven that areal analysis has a smaller variation than lineal traverse or random point counting [14]. Systematic point counting is more efficient than areal analysis, but the validity of systematic point counting is based on two assumptions: First, the objects must be more or less spherical. Second, the size distribution of the objects must not have any gaps [14]. Often these two assumptions have been ignored in practice. Thus, areal analysis remains the most accurate, and generally applicable, procedure.

Since a digital image is composed of pixels, or image points, the basic operation of the automatic measurements by a computer is counting the relevant image points. Computer image analysis can easily perform an areal analysis by counting all pixels and the pixels within the objects. Therefore, the estimation of volume fraction can be more accurate with computer image analysis. Since the pixels are close-packed, such an areal analysis is equivalent to

performing many close-packed lineal traverses, or even more close-packed point countings.

Many image analyzers are not specially designed for the quantitative microscopy of materials. Manual examination may still have its advantages over some of these image analyzers. For example, the process of image segmentation is a critical step in image analysis, because all measurements are completely dependent on the segmentation results. During manual examination, the process of image segmentation is an intuitive process. Humans can instantly recognize objects from background. Computer recognition of objects from background has been the topic of many books. There are several common methods for segmenting an image that are not specially designed for quantitative image analysis [15,16]. Quantitative image analysis requires more accurate segmentation than non-quantitative image analysis.

Another intuitive process in manual examination is object selection and counting. This is also very difficult for some automatic image analysis systems [17] because it involves the process of individual object labeling. Sometimes geometric properties such as the areas and perimeters of individual objects are desired. These individual measurements are very time consuming for manual examination. For some image analyzers which are less capable of object selection, they are also difficult or impossible.

The current research work has developed an automatic quantitative image analysis (AQIA) software system specially designed for materials' analysis. It is implemented on an UNIX operating system with a Tektronix graphics terminal as a monitor. Compared with many image analyzers, it is almost hardware independent. With a few changes, it can be run on any UNIX operating system with any high resolution monochromatic monitor. With some additional changes it can also be transported to a microcomputer with an appropriate graphic terminal. Therefore, it is much less expensive than the existing hardware-type automatic image analyzers. It is specially developed for quantitative microscopy of construction materials.

The resolution of AQIA is the resolution of the digitizer divided by the magnification of microscope in use. The high resolution digitizer that has been used in this work can divide an image into pixels that are 25 μm wide. If the image has been magnified by 100X, then each pixel represents 0.25 μm on the actual object. That means AQIA can measure easily either small objects or small features on larger objects.

This system tries to combine the advantages of manual examination and automatic image analysis. It has some unique features. It not only uses areal analysis to estimate volume fraction, but also helps the user design experiments for volume fraction estimation. That is, it

helps one to select the number of images and image size to meet a desired estimation accuracy, or predict an accuracy associated with an affordable effort with a given number of images of a given size.

It simulates the process of human segmentation and object counting to make these two automatic processes more realistic. It labels objects to make individual measurements easy. With labeled objects, AQIA can process an image more accurately and with more flexibility than can a non-labeling analysis system. Because the reliability of image measurement depends on the accuracy of image segmentation and processing, AQIA is expected to provide more reliable measurements.

Another unique feature of AQIA is its method of estimating the spatial size distribution of particles in a matrix. The estimation of the size distribution usually needs the assumption that the particles are spheres. This assumption is too restrictive. AQIA uses a completely different approach to attack this problem. It can estimate the spatial size distribution of particles of any given shape, as long as the shape can be modeled by a computer.

AQIA can have a variety of specific applications to cement and concrete research. Image analysis may be the only reliable technique for some measurements such as the distribution of big pores in concrete and the flyash size

distribution. AQIA can provide solutions to these kinds of difficult measurements. However, the aim in the development of the AQIA system has been to produce a package of programs that are generally applicable to the broad spectrum of construction materials research. Thus, specialized programs that produce only one result have been avoided. It is hoped that this has produced a package that will be broadly applicable to researchers.

DESIGN OF EXPERIMENTS IN VOLUME FRACTION ESTIMATION

Interval Estimation of Volume Fraction

In quantitative microscopy, the volume fraction estimation is probably the most frequently performed analysis. In AQIA, the volume fraction is estimated by using an areal analysis performed on images of sections cut through the material. The first step must be the experimantal design: selecting the number of images and the size of each image to meet a desired estimation accuracy or, calculating the obtainable accuracy with a given number of images of a given size that comprises an affordable effort. This section describes this design process.

Areal analysis in manual examinations is exceedingly rare because of the experimental difficulties. Further, there are usually no discrete images, or fields of view, during manual examination. The sample is typically in continuous motion with respect to the observer. In a computer image analysis system, one uses one or more separate images and examines everything lying within them. Hence, the estimation of the accuracy of a measurement is different. What follows is a method specially designed for

computer image analysis systems.

The coefficient of variation among area fraction measurements can be determined by the average number of intercepted objects per image as [14]: (See Appendix B)

$$\frac{\sigma(A_A)}{\overline{A_A}} = \left| \frac{\frac{\sigma^2(a)}{(\bar{a})^2} + 1}{\overline{M_a}} \right|^{0.5} \qquad (1)$$

where $\overline{M_a}$ is the average number of intercepted objects per image and $\sigma^2(a)/(\bar{a})^2$ is the squared coefficient of variation of the areas of the intercepted objects. This squared coefficient of variation can be shown to be 0.2 for spheres and bigger for other shapes (See Appendix C). It can be measured experimentally. $\overline{A_A}$ is the mean value of area fractions obtained from a number of equal-size images, and $\sigma(A_A)$ is the standard deviation among these area fractions. Thus, $\sigma(A_A)/\overline{A_A}$ is the coefficient of variation among area fractions. For the example of spherical objects, a 5% coefficient of variation requires that $\overline{M_a}$ = 480, while 10% requires only 120 objects per image. If the dispersed phase is widely separated, as, for example, the air voids in concrete, a large image is needed to include sufficient objects for a low coefficient of variation. It is impractical to prepare and store in a computer a large image. Even if it is possible, from the view point of statistical estimation, Eqn. 1 only indicates the

dispersion among area fraction measurements, it does not directly indicate the accuracy of the volume fraction estimation. One must use statistical interval estimation to obtain the volume fraction accuracy.

From the view point of the statistical interval estimation, a three-dimensional specimen of interest can be considered as a population of an infinite number of sections. The volume fraction is the average of all the area fractions from the infinite number of sections. The distribution of all these area fractions can be reasonably considered as a normal distribution having the volume fraction as the population mean and an unknown but finite variance. In practice, it is impossible to obtain all these area fractions. Therefore, the volume fraction must be estimated from the measurements performed on a limited number of sections.

In terms of volume fraction analysis, we specify the volume fraction, V_V, as the population mean, the number of images, n, as the sample size, the mean area fraction, $\overline{A_A}$, as the mean of the sample distribution, the area fraction from each image, A_A, as the measurement (random variable), the variance among the area fractions, $\sigma^2(A_A)$, as the variance of the sample distribution, and the variance among the mean area fractions, $\sigma^2(\overline{A_A})$, as the variance of the sampling distribution. According to the principles of interval estimation [18], we have:

$$\sigma^2(\overline{A_A}) = \sigma^2(A_A)/n, \qquad (2)$$

and

$$\overline{A_A} - \text{half-width} < V_V < \overline{A_A} + \text{half-width} \qquad (3)$$

Because the population variance is unknown, the half-width, or the error of estimation, is related to Student's t-distribution, instead of a normal distribution [18]. The half-width is given by:

$$\text{half-width} = t_{(1-\alpha/2,n-1)} \times \sigma(\overline{A_A}) \qquad (4)$$

or:

$$= t_{(1-\alpha/2,n-1)} \times \frac{\sigma(A_A)}{n^{0.5}}$$

where $1 - \alpha$ is the confidence level, and $t_{(1-\alpha/2,n-1)}$ is the $100(1 - \alpha/2)$ percentile of the t distribution with $n - 1$ degrees of freedom.

This kind of inference that we may make in terms of confidence intervals is illustrated in Fig. 1. The horizontal line represents the fixed value of the population mean (V_V). The vertical lines represent possible intervals generated by successive random samples of size n and with confidence level $1 - \alpha$. The middle point of each vertical line represents the sample mean ($\overline{A_A}$). The half length of each vertical line represents the half-width of the interval, so that the upper and lower ends of each vertical line represent the values of $\overline{A_A}$ + half-width and $\overline{A_A}$ -

half-width respectively. As Eqn. 3 and 4 show, the value of $\overline{A_A}$ and $\sigma(\overline{A_A})$ may be different for different samples. Therefore, the half-width and the sample mean ($\overline{A_A}$) may be different. This means that the vertical positions and the lengths of the vertical lines are variables. Some of the vertical lines may not intercept the horizontal line, i.e., the intervals may not contain the population mean. A $1 - \alpha$ confidence level means that $1 - \alpha$ of all possible vertical lines will intercept the horizontal line, i.e., $1 - \alpha$ of all possible intervals will contain the population mean. In practice, of course, we never select more than one sample from a population. Based on this one sample mean, ($\overline{A_A}$), we establish a confidence interval.

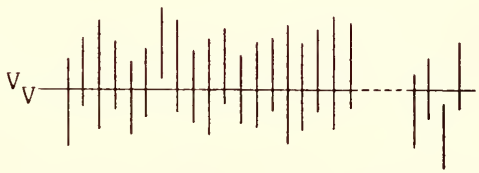

Figure 1

Illustration of Confindence Intervals

Predication of Estimation Accuracy

Because the coefficient of variation is the standard deviation divided by the mean, if the mean, $\overline{A_A}$, can be obtained from a pilot experiment performed on a small sample, or from experience, and $\overline{M_a}$ is known, the standard

deviation of the sample distribution, $\sigma(A_A)$, can be found from Eqn. 1. This equation can be rewritten as:

$$\sigma(A_A) = \left| \overline{A_A} \times \frac{C}{\overline{M_a}} \right|^{0.5} \qquad (5)$$

where C is $1 + \sigma^2(a) / (\overline{a})^2$. C = 1.2 for spheres and is bigger for other shapes. Equation 5 can be substituted into equation 2 to calculate the standard deviation of the sampling distribution in advance of the full-scale experiment with n sections, as:

$$\sigma(\overline{A_A}) = \overline{A_A} \times \left| \frac{C}{n \times \overline{M_a}} \right|^{0.5} \qquad (6)$$

Once the standard deviation of the sampling distribution is available, the error of estimation can be found in terms of the half-width of the interval as:

$$\text{half-width} = t_{(1-\alpha/2,n-1)} \times \sigma(\overline{A_A}) \qquad (7)$$

or:

$$= t_{(1-\alpha/2,n-1)} \times \overline{A_A} \times \left| \frac{C}{n \times \overline{M_a}} \right|^{0.5}$$

Design of Experiments

Eqn. 7 shows that the estimation accuracy at a given confidence level, indicated by half-width, is affected not

only by $\overline{M_a}$, the average number of the intercepted objects per image, but also by n, the number of images. The experimenter may know the values of n and $\overline{M_a}$ that are fixed by experimental conditions. Therefore the estimation accuracy can be calculated.

On the other hand, if we want to meet a desired estimation accuracy at a given confidence level, we can select n and $\overline{M_a}$ to satisfy:

$$t_{(1-\alpha/2,n-1)} \times \overline{A_A} \left| \frac{C}{n \times \overline{M_a}} \right|^{0.5} \leq \text{half-width} \qquad (8)$$

where $\overline{A_A}$ is obtained from a pilot experiment or experience. If Eqn. 8 is rewritten into:

$$\frac{t_{(1 - \alpha/2,n - 1)}}{n^{0.5}} \leq \frac{\text{half-width}}{\overline{A_A}} \times \left| \frac{\overline{M_a}}{C} \right|^{0.5} \qquad (9)$$

and if $\overline{M_a}$ is set, then the right side is a constant, and n can be found by searching the t-table (Appendix D) to fit Eqn. 9. For example, suppose C = 1.2, $\overline{A_A}$ = 0.1, the half-width is desired to be 0.01, the confidence level is desired to be 0.95, and $\overline{M_a}$ = 100, n turns out to be at least 8. Obviously, if n is set, $\overline{M_a}$ can also be figured out.

Eqn. 8 may also be rewritten as:

$$\frac{t_{(1 - \alpha/2,n - 1)}}{\left| n \times \overline{M_a} \right|^{0.5}} \leq \frac{\text{half-width}}{\overline{A_A} \times C^{0.5}} \qquad (10)$$

Assuming that $\overline{A_A}$ has been obtained from a pilot experiment and the desired values of half-width and α have been selected, a compromise can be made between n and $\overline{M_a}$, to meet the desired accuracy. For example, if $\overline{A_A}$ = 0.1, half-width = 0.01, and 1 - α = 0.95, then this relation between n and $\overline{M_a}$ is shown in Fig. 2.

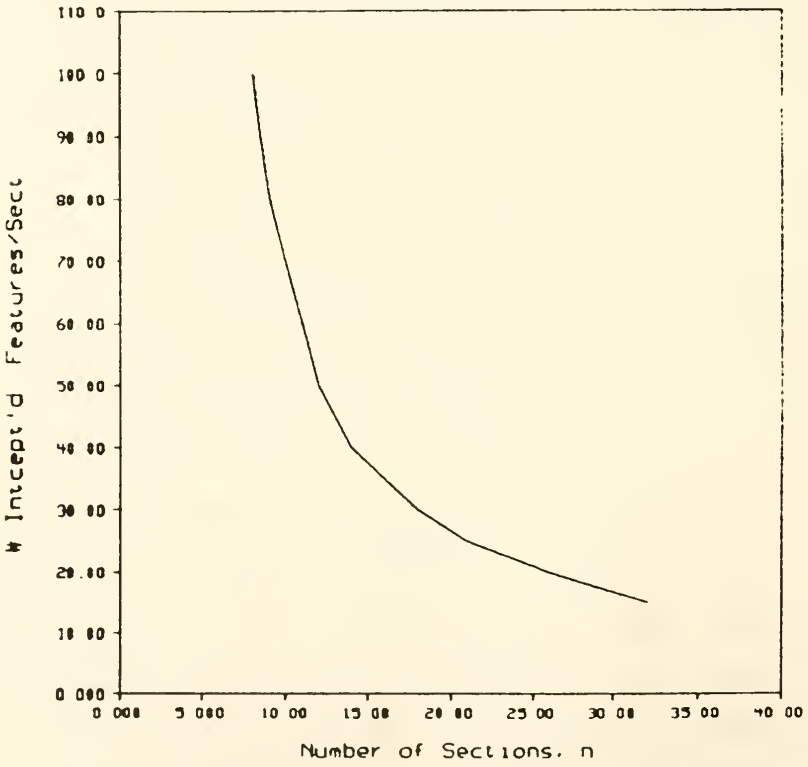

Figure 2

Size of Sections vs. the Number of Sections

Fig. 2 indicates that many combinations of n and $\overline{M_a}$ will

achieve the same accuracy. For instance, if $\overline{M_a} = 100$, then at least 8 images are required. This combination may be impractical. If $\overline{M_a} = 20$ is practical and the other parameters remain the same, the sample size turns out to be at least 26. This means that either 8 images with 100 intercepted objects per image, or 26 images with 20 intercepted objects per image can provide the same estimation accuracy in this case.

One might consider that the product of n and $\overline{M_a}$ indicates the total effort for the estimation. It is found that the total effort decreases as n increases. Eqn. 9 can also be rewritten as:

$$n \times \overline{M_a} \geq \left| \frac{t_{(1 - \alpha/2, n - 1)} \times \overline{A_A}}{\text{half-width}} \right|^2 \times C \qquad (11)$$

If one assumes a given half-width, that $\overline{A_A}$ is obtained from some pilot experiment and C = 1.2, then Eqn. 11 becomes:

$$n \times \overline{M_a} \geq t_{(1 - \alpha/2, n - 1)}^2 \times \text{constant} \qquad (12)$$

The factor $t_{(1-\alpha/2, n-1)}$ decreases as n increases (See Appendix D). Fig. 2 shows that, for a given accuracy, if n increases, $\overline{M_a}$ decreases a great deal. Therefore, for a given accuracy, the product of n and $\overline{M_a}$ decreases as n increases. For example, if $\overline{A_A} = 0.1$, half-width = 0.01, and $1 - \alpha = 0.95$, this relation between n and $n \times \overline{M_a}$ is shown in Fig. 3.

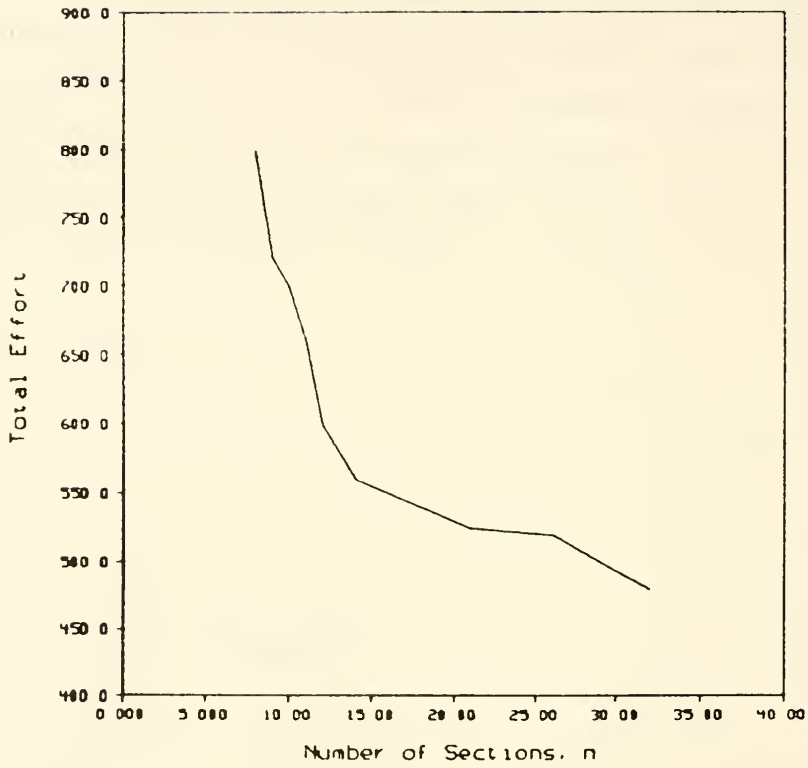

Figure 3

Total Effect vs. the Number of Sections

It follows that, for a given accuracy, a larger number of images will allow a smaller $\overline{M_a}$, and a less total effort. Unfortunately, during microscopic observations, $\overline{M_a}$ is usually fixed by the magnification of the image. For the example of air void measurement in concrete, assuming the smallest air voids are 2 μm, and the resolution of the digitizer is 25 μm, we need to select a magnification such that the AQIA system will 'see' all the

air voids, but not 'see' finer pores. In this case, the resolution of the AQIA system may need to be 1 μm. The resolution of the AQIA system is the resolution of the digitizer divided by the magnification of the microscope, therefore the rational choice of the magnification may be 25X. Once the magnification is given, we have almost no choice for the field of view that fixes $\overline{M_a}$. This means that we have almost no choice for $\overline{M_a}$. Therefore, for real applications, only n, the number of images (fields of view) can be changed.

To sum up, for microscopic measurement, the magnification of the microscope should be selected first to provide a resolution for the AQIA system so that all objects of interest can be 'seen', but no finer objects can. This magnification determines $\overline{M_a}$. Then using Eqn. 9, a value of n can be found to meet the desired accuracy.

A large n means a big effort. We may need to adjust the confidence level, or estimation accuracy, to make the effort affordable. Table 1 is an example showing how different confidence levels and estimation accuracies can affect n, for $\overline{A_A}$ = 0.1 and $\overline{M_a}$ = 10. Other values of $\overline{A_A}$ and $\overline{M_a}$ would produce other values of n for the various accuracies.

This table shows that reduction of either accuracy or confidence level can reduce the number of required images.

Table 1

Number of Required Images, n

accu. \ conf. level	0.95	0.90
0.01	48	34
0.02	14	11
0.03	8	6
0.04	6	5
0.05	5	4

For example, if the accuracy is desired to be 0.01, i.e, the value of the volume fraction must be known within the range 0.09 to 0.11, then a change of the confidence level from 0.95 to 0.90 can reduce the number of images from 48 to 34. Of course, this reduces the confidence one has in the answer. If the confidence level is desired to be 0.95, a change of the desired accuracy from 0.01 to 0.05 can reduce the number of images from 48 to 5.

AQIA has a procedure called "design", that allows the user to find the value of n, given the image size ($\overline{M_a}$), the estimated mean value of the area fraction ($\overline{A_A}$), the desired estimation accuracy (half-width) and the desired confidence level ($1 - \alpha$). To use "design", the user should obtain $\overline{A_A}$, either from a pilot experiment or from experience; and select a desired accuracy (half-width) and

a confidence level. The user must also know the approximate value of $\overline{M_a}$ for the appropriate magnification and sample. After the user enters the values of $\overline{A_A}$, half-width, $1 - \alpha$ and $\overline{M_a}$, the program will find the value of n. If the user is not satisfied with the result, because n is too large, he/she can change any one of these four values. This will usually involve compromising on the accuracy. The new values can then be re-entered until he/she obtains a value for n that is experimentally feasible.

SEGMENTATION OF DIGITAL IMAGE

Before displaying or processing a digital image, frequently it must be segmented into a binary image. This is because a monochromatic monitor can only display binary information: e.g. ´on´ points and ´off´ points. Also, further processing is much easier with a segmented image. Image segmentation is the critical step in quantitative image analysis, because all measurements are performed on the binary image.

Gray level histogram thresholding is a widely used tool in image segmentation. AQIA has a program called ´histo´ to calculate a histogram of the occurrence of various gray levels. A lower bound and an upper bound can be selected from this histogram of gray levels. All the gray levels within the bounds are then assigned gray level = 1. All the gray levels beyond the bounds are made = 0. This results in a binary image. The points with gray level 1 are illuminated on the screen while gray level 0 points are left dark.

These bounds may be selected manually from the histogram. AQIA has a program called ´bitshow´, that asks the

user to enter the selected bounds and displays the resulting binary image on the screen. It allows the user to keep changing the bounds until the user is satisfied with the image. Fig. 4 shows a photograph taken of a sample of several particles of quartz. When it is digitized, Fig. 5 shows the resulting histogram of 256 gray levels (0 - 255). Fig. 6 is the expanded lower part of Fig. 5. The largest values of the gray levels represent the particles and the smallest values are the background. An upper bound of 255 would be a logical selection. The lower bound must lie between the two peaks at 0 and 255. But, it is difficult to tell the exact location of the lower bound. Different users, or the same user at different times, might select a different lower bound. Thus, manual thresholding may not be consistent. Slight inconsistencies may not affect the calculation of volume fraction significantly, but, the surface area and the spatial size distribution of the objects will be greatly affected. Therefore, one needs a consistent, automatic threshold selection that is based on some rational evaluation criteria.

Currently Used Automatic Threshold Selections

Gray level thresholding is essentially a classification problem. A typical bimodal image contains dark objects on a light background or vice versa. Its gray

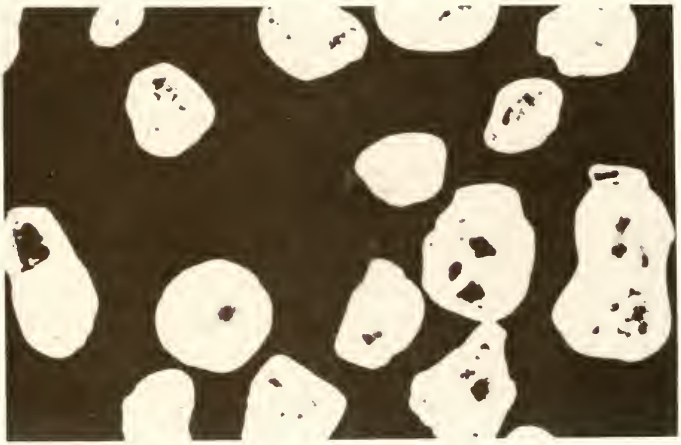

Figure 4

Original Image of Quartz

level histogram contains two peaks, representing the populations of objects and the background phase, separated by a valley corresponding to the intermediate gray levels. The object of thresholding is to classify these intermediate gray levels as having a membership in one of the two phases. An optimal threshold should minimize the probability of misclassifying an object point as background or vice versa. If the object and background distributions are known, the optimal threshold can be obtained in terms of

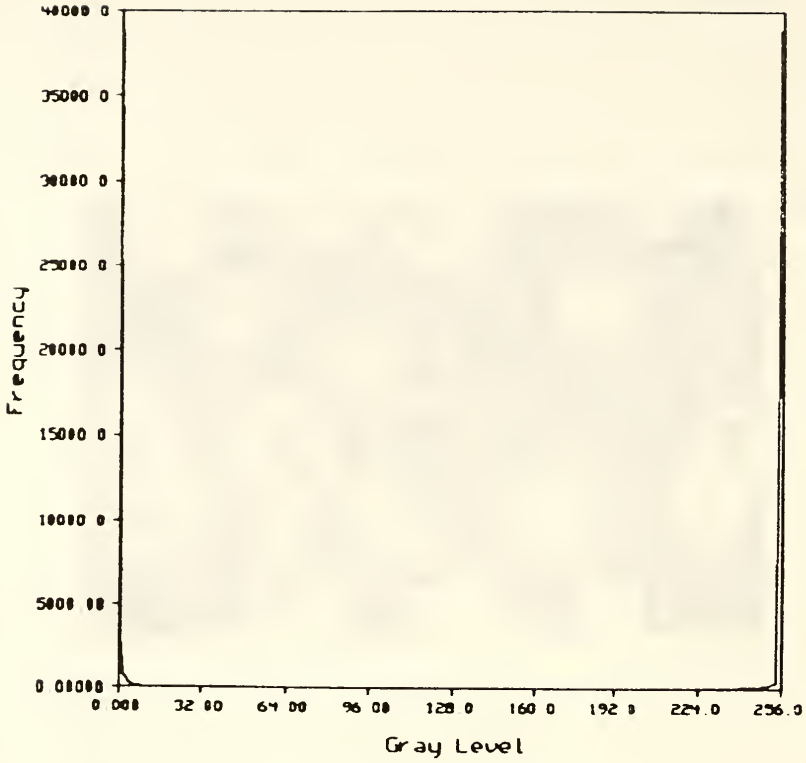

Figure 5

Complete Histogram of Gray Level (Quartz)

these two distributions' parameters [16, 19, 20]. Unfortunately, these two distributions are usually unknown. Therefore, generally, they can not be used to automatically threshold an image.

A threshold can also be evaluated by a 'busyness' measure performed on the digital image. 'Busyness' is the number of adjacencies between above-threshold and below-threshold points [16, 21, 22]. 'Busyness' is the sum of

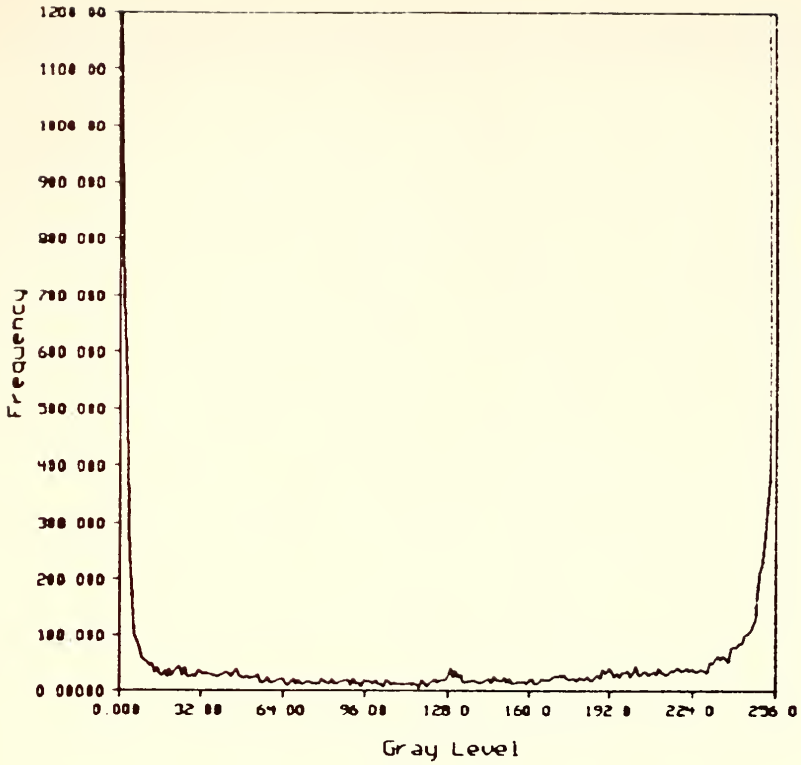

Figure 6

Enlarged Histogram of Gray Level (Quartz)

the absolute values of each point's Laplacian calculated on the thresholded image. The Laplacian value at a point (i,j) is:

$$\nabla^2(i,j) = g(i+1,j) + g(i-1,j) + g(i,j+1) + g(i,j-1) - 4 \times g(i,j) \quad (13)$$

where g(i,j) is the gray level of point (i,j). The Laplacian is proportional to the number of neighbors that have different gray level from the point (i,j). Intuitively, a high 'busyness' would indicate that the binary image has a

large number of boundary points. This means a large number of very small objects and/or jagged boundaries.

In non-quantitative image analysis cases, the very small objects are usually considered to be noise, and the boundaries of objects are usually assumed smooth. Therefore, high 'busyness' usually indicates bad thresholding. An optimal threshold should minimize the 'busyness' provided that the thresholding does not classify all the gray levels into the same binary level. However, this method may not work well in quantitative image analysis cases. In quantitative image analysis, it is very likely that there will be very small objects and objects with jagged boundaries in the image that are of interest. Thus, minimization of 'busyness' can not be used.

There are also a variety of techniques that enhance an image or modify its histogram, in order to make the threshold selection easier [24-27]. These techniques can make two peaks more separate if they overlap, or make a valley between peaks deeper if it is broad and/or flat. However, they only modify the histogram. The threshold selection is still not automatic nor necessarily consistent.

Basic Concepts of Fuzzy Sets and Their Application

Recently, the concepts of fuzzy set theory have been applied to threshold selection. As mentioned early, the task of thresholding is to classify the intermediate gray levels. These intermediate gray levels come primarily from boundary points. In any real picture, the precise boundary between an object and the background is usually ill defined, or 'fuzzy'. Therefore, it seems quite natural to apply concepts of fuzzy set theory to threshold selection.

Let X = [x] denote a sample space. For example, X could be a set of some integers between 1 and 10:

$$X = [\ 1,\ 1,\ 2,\ 3,\ 3,\ 4,\ 5,\ 5,\ 6,\ 8,\ 9,\ 9,10\ ].$$

Let A denote a subset in X. For example A could be:

$$A = [\ 5\ ].$$

Subset A is an ordinary subset. Any integer is either in subset A or it is not. No intermediate, or 'fuzzy' status exists.

However, a subset is often ill defined. Then A is defined as a fuzzy subset in X. A fuzzy subset is defined by:

$$A = [\ x/\ \mu_A(x)\ ].$$

where $\mu_A(x)$ is termed 'the degree of membership of x in A'. For example, A could be 'a few'. 'A few' is a fuzzy

definition. It is likely to mean 3 or 4, and unlikely to mean 8 or greater. Therefore, the fuzzy subset A might be:

$$A = [\ 1/0.0,\ 2/0.5,\ 3/1.0,\ 4/1.0,\ 5/0.8,$$
$$6/0.4,\ 7/0.2,\ 8/0.0,\ 9/0.0,\ 10/0.0\ ].$$

This means, for example, that the degree of membership of integer 5 in subset 'a few' is 0.8, or the degree of belief that integer 5 belongs to 'a few' is 0.8.

An image can be considered as a set of points, I, each point x being associated with a certain light intensity, or gray level i, as:

$$I = [x_i]$$
$$= [\text{ point x with gray level i }].$$

The gray levels normally range from 0 to 255. Thresholding will classify all the points into two subsets: the object subset and the background subset. The boundary between these two subsets is often ill defined, or 'fuzzy'. Thus, the object subset and the background subset are fuzzy subsets in this case. Consider the object subset as an example. It is a fuzzy subset O:

$$O = [\text{ object point }]$$
$$= [\ x_i\ /\ \mu_O(x_i)\ ]$$

where x_i is a point with gray level i and $\mu_O(x_i)$ is its degree of membership in object subset O. The basic idea of applying fuzzy set theory to image segmentation [28-32] is that the different gray levels have different degrees

of membership in the object subset. Some 'standard' function with two or more parameters is used as the membership function to give the degree of membership of the various gray levels. A cross-over gray level is selected, located in the valley of the histogram of gray levels. By definition, the points with a cross-over gray level have a 0.5 degree of membership in the object subset, or:

$$\mu_0(x_{\text{cross-over}}) = 0.5$$

Different cross-over gray levels will give different segmentation results. Different parameters of the membership function will also affect the image segmentation differently. The optimal threshold should minimize a 'fuzziness' measure [31]. The 'fuzziness' measure reflects the closeness between a digital image and a binary image, or the image ambiguity. But, this criteria has not proven to be sufficient. If both the cross-over point and the parameters of the membership function change, their individual effects on the 'fuzzyness' measure may cancel each other. In other words, different cross-over points may give the same 'fuzzyness' measure. Also, this method has the same trouble as many other threshold selection techniques. If there is a broad and flat valley between the peaks, there will be too many candidates for the cross-over point.

AQIA Approach

In quantitative image analysis, one criterion for the reliability of image thresholding selection might be the accuracy of the measurements made on the thresholded image. However, generally the "right" answer is unknown. Hence, the accuracy can not be defined. Thus, this criterion is not applicable. However, during manual examinations, a human can instantly differentiate objects from background using intuition. AQIA uses the concepts of fuzzy probability to simulate the cognition process of a human's segmentation to improve the reliability of the segmentation.

First, reconsider the subset problem. If we have an ordinary subset A = [5] of the example set of integers, the probability of event A occuring in X is 2/13. (Two 5's in the set of 13 members) But, if the subset A is the fuzzy subset 'a few', defined as

A = [1/0.0, 2/0.5, 3/1.0, 4/1.0, 5/0.8,
6/0.4, 7/0.2, 8/0.0, 9/0.0, 10/0.0].

what is the probability that the fuzzy event A, "a few", occurs in X? Zadeh has provided a framework to give a probability measure of a fuzzy event [33]. In the discrete case, the probability measure of a fuzzy event A is expressed by:

$$p(A) = \sum_{i}^{n} \mu_A(x_i)\ f(x_i)\ . \qquad (14)$$

where n is the number of elements in set X, $\mu_A(x_i)$ is the degree of membership of x_i in A and $f(x_i)$ is the ordinary probability that x_i occurs in X. For the above example, the fuzzy probability of event A, "a few", in X is

$$\begin{aligned} p(A) &= 0.0 \times \frac{2}{13} + 0.5 \times \frac{1}{13} + 1.0 \times \frac{2}{13} \\ &\quad + 1.0 \times \frac{1}{13} + 0.8 \times \frac{2}{13} + 0.4 \times \frac{1}{13} \\ &\quad + 0.2 \times \frac{0}{13} + 0 \times \frac{2}{13} + 0 \times \frac{1}{13}. \\ &= \frac{0.5 + 2.0 + 1.0 + 1.6 + 0.4}{13} \\ &= 0.42 \end{aligned} \qquad (15)$$

This value, 0.42, is the probability that a number in the set X will also be in the fuzzy subset 'a few'. Assume an image has dark objects on a light background, and the histogram has two peaks with maximums at gray levels 0 and 255. As mentioned early, 'object' or 'dark' is considered as a fuzzy subset O:

$$\begin{aligned} O &= [\ \text{object point}\ ] \\ &= [\ x_i\ /\ \mu_O(x_i)\ ] \end{aligned}$$

What is the probability that the fuzzy event, 'object' or 'dark' point, appears in an image set I? Or, what is the probability that a point in I is an object point? Or, what is the probability that a point in I is dark? The answer is:

$$p(O) = \sum_{i}^{n} \mu_O(x_i)\ f(x_i) \qquad (16)$$

where n is the total number of points in the image, and $f(x_i)$ is the relative frequency of gray level i that can be obtained from the gray level histogram. $\mu_0(x_i)$ is the degree of membership of gray level i in the 'dark', or object, subset. Obtaining $\mu_0(x_i)$ will be discussed later.

Consider next the physical interpretation of p(0). It is the area fraction of the object phase in the image, because the probability that an object point appears in image I is just the area fraction of objects in the whole image. Or:

$$p(0) \equiv \text{Area Fraction of Objects} \tag{17}$$

Assuming that $\mu_0(x_i)$ is available, and that the relative frequency of each gray level, $f(x_i)$, is already obtained from the gray level histogram, the area fraction of the object phase is readily calculable from Eqn. 16. Thus one calculates the area fraction before thresholding. This calculation is based on a prior knowledge of the membership function, or, on a knowledge of the degree of membership of a gray level in the subset 'object'. Once the area fraction is determined, the gray level threshold on the histogram can be located. It should divide the whole area below the histogram curve into two parts, the area of one part being p(0) of the whole area and the area of another part being 1 - p(0) of the whole area.

Construction of the Membership Function $\mu_0(x_i)$

The fuzzy approach used here is critically dependent upon a knowledge of the degrees of membership of the gray levels in the subset 'object'. Therefore, it is not sufficient to use a 'standard' membership function. One must be determined experimentally for this specific application. The pairwise comparison method [34] was employed to establish the membership function $\mu_0(x_i)$. Seven paint samples of different gray levels from Pittsburgh Paints were shown to the observers a pair at a time. Fig. 7 shows these seven paint samples and their manufacturing code numbers. The darkest and lightest samples were displayed as extremes. Five persons were used as observers. They assessed how much one of a pair was darker than the another one according to a specially designed questionaire (See Appendix E). A numerical scale (1 - 7) was used to assign a value to the relative strength of the darkness. Comparisons were repeated for all pairs from these seven paint samples. The averages of the five observers' assessments for each pair were taken as the relative strength. Since there were 7 grays, a 7 x 7 non-symmetric full matrix of relative darkness was formed. The degrees of membership of these seven grays in the 'dark' subset are the eigenvector corresponding to the maximum eigenvalue of the matrix.

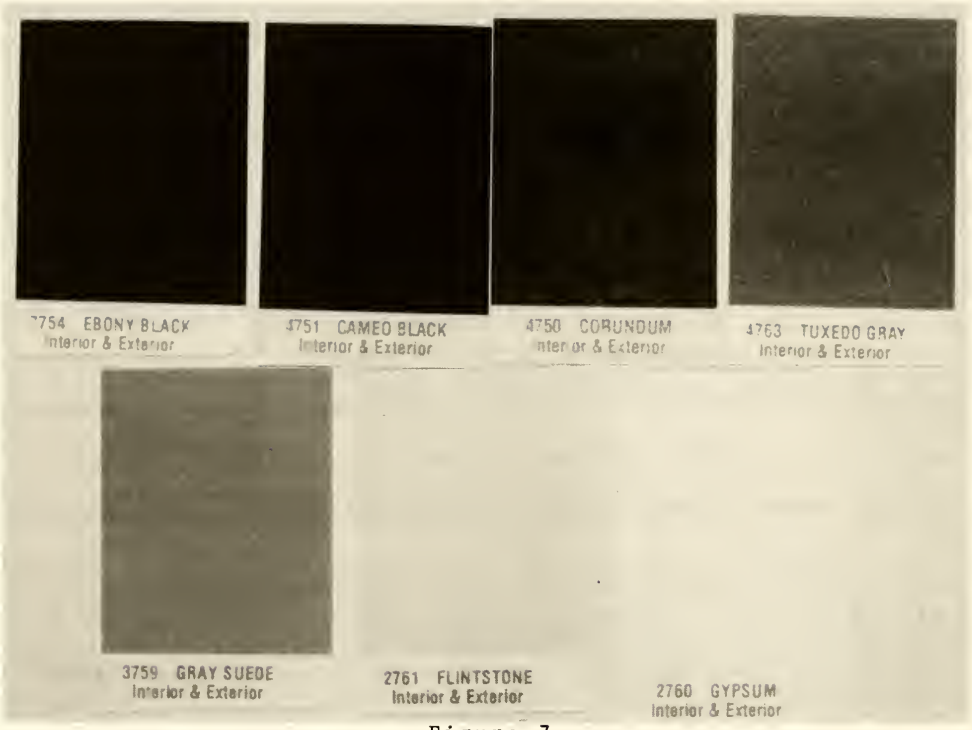

Figure 7

Paint Samples

The seven grays range from white to black. They were photographed and the resulting negative was used to determine the gray levels with a digitizer. The seven gray colors have gray levels 240, 229, 214, 199, 163, 82 and 41 respectively. The digitizer assigned 0 to an ´opaque´ (extremely dark) gray and 255 to a ´transparent´ (extremely light) gray. The transparent part on a negative should be the extremely dark part of the original image, and the opaque part on a negative should be the

extremely light part on the image. Therefore, if a negative is digitized, 255 corresponds to the extremely dark part on the original image, and 0 the extremely light part. From now on, we assume that negatives will be digitized, so that gray level 255 has 1.0 degree of membership in 'dark' subset, and 0 has 0 degree of membership. Because 240 is close to 255, it is reasonable to assume 240 as extremely dark, or gray level 255. But it is not wise to treat 41 as 0 because the paint sample with gray level 41 looks far from transparent. Therefore, the measured gray levels were shifted so that 240 became 255 and 41 became 56.

Table 2 shows the 7 x 7 matrix of relative darkness of these seven grays. The maximum eigenvalue is 7.60325, the corresponding eigenvector is: (0.0177, 0.0298, 0.0474, 0.0843, 0.1232, 0.2021, 0.2359). These seven values were then converted into a scale that ranges from 0.0 to 1.0. This was done by shifting them all along the scale so that the smallest became 0.0. Then they were normalized so that the largest became 1.0. The new vector becomes: (0.0, 0.056, 0.136, 0.305, 0.484, 0.845, 1.0). Table 3 shows the degrees of membership of these seven grays in 'dark' subset. All the gray levels below 56 are assumed to have a 0.0 degree of membership.

An index of consistency has been suggested to evaluate experimental results in pairwise comparisons. It is

Table 2

Experimental Data of Relative Darkness

Paint Sample	1	2	3	4	5	6	7
1	1.00	3.25	4.75	5.50	6.00	7.00	7.00
2	0.31	1.25	2.50	4.50	5.25	5.25	6.00
3	0.21	0.40	1.60	3.50	3.25	4.50	5.00
4	0.18	0.22	0.29	1.25	3.00	4.00	3.50
5	0.17	0.19	0.31	0.33	1.00	3.00	3.00
6	0.14	0.19	0.22	0.25	0.33	1.00	1.75
7	0.14	0.17	0.20	0.29	0.33	0.57	1.00

defined [34] by:

$$I_c = \frac{\lambda_{max} - n}{n - 1} \tag{18}$$

where I_c is the index of consistency, λ_{max} is the maximum eigenvalue, and n is the number of objects (grays). When $I_c = 0$, the assessments of each observer are completely consistent. A larger I_c means less consistency. In the current experiment, the index of consistency is 0.1. The deviation of the diagonal values of the matrix from 1.0 also indicates the inconsistency. Among the seven values, there are four 1's, two 1.25's and one 1.60.

Fig. 8 shows a smooth curve that has been fit to the experimental data. It is a fourth order orthogonal polynomial function, and is given below with i being the gray

Table 3

Degrees of Membership of Gray Levels in 'Dark'

Gray Level i	Membership $\mu_0(x_i)$
255	1.000
244	0.845
229	0.483
214	0.305
178	0.136
97	0.056
56	0.000

level:

$$\mu_0(x_{56<i<255}) = -2.33694 \times 10^{-2} - 2.53554 \times 10^{-3}\, i + 8.64525 \times 10^{-5}\, i^2 - 7.12423 \times 10^{-7}\, i^3 + 1.86732 \times 10^{-9}\, i^4 \qquad (19)$$

and:

$$\mu_0(x_{255}) = 1.0$$
$$\mu_0(x_{i\leq 56}) = 0$$

Using this membership function and Eqn. 16, the histogram in Fig. 5 was thresholded at gray level 181. (The other bound is 255). Fig. 9 shows the corresponding binary image. Comparing Fig. 4 and Fig. 9 shows that the thresholded image is a good representation of the original

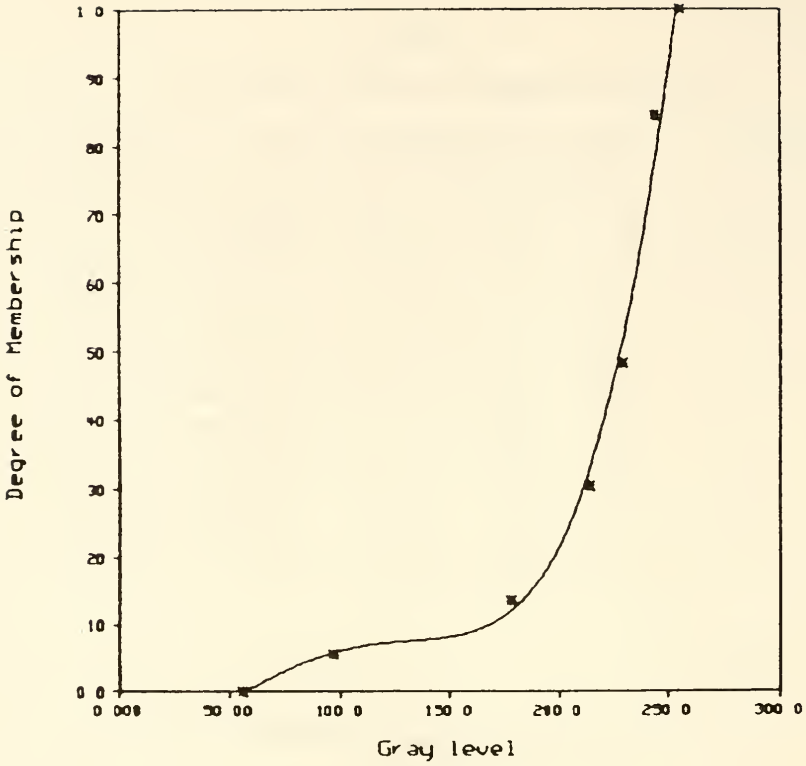

Figure 8

Membership Function of Gray Levels in `Dark´ Subset

image.

When a human tries to differentiate objects from background, he/she must consider the relative darkness of the image points. This method models this aspect of a human´s cognition process of classifying intermediate gray levels into ´dark´ and ´light´ subsets. Therefore, this method is expected to work at least as well as manual threshold selection. Its big advantage over the manual selection is that it is consistent. Different operators

Figure 9

Binary Image of Quartz

will always threshold the same image in exactly the same way if they use the same membership function.

General Use of the Fuzzy Probability Thresholding

Up to this point,, the histogram has been assumed to have two peaks at 0 and 255 respectively. In other words, the two extremes are ´extremely dark´ and ´extremely light´. The fuzzy membership experiment is designed for this special case. However, sometimes a peak or peaks will appear at other points along the gray level scale. It is impractical to obtain the membership function for each case by experiment. A simple normalization is used in this work to solve this problem. If two peaks have maxima at gray levels p1 and p2 (p2 > p1) respectively, p1 and p2 can be assumed as extremes. The segment between p1 and p2

can be normalized into a 0 - 255 scale. Using Eqn. 19, the degree of membership of each gray level between p1 and p2 can be determined. If the area between these two peaks is considered as unity, the value of p(0) can be calculated from Eqn. 16. Then, a threshold can be found between p1 and p2. Furthermore, if an image has more than two peaks, the degrees of membership can be determined for each gray level between any two peaks, with these two peaks as extremes. Then gray levels between these two peaks can be thresholded. AQIA has a program called 'fuzzythr', that asks the user to enter any two peak gray levels between which a threshold is to be located. Then the program will find the location of that threshold.

A disadvantage of this method is that it can not be applied to a unimodal image. If the histogram has only one peak, this peak can be considered as an extreme. But, lacking another extreme, the scale can not be normalized. However, bimodal or multi-modal images are much more likely to appear in quantitative image analysis than unimodal images. Therefore, this general method may be useful for thresholding many images for quantitative analysis use.

Edge-detection

AQIA also has an edge-detection procedure [38] that singles out the boundaries of objects. Gray levels are relatively consistent within each of the two phases, and change abruptly as the border between the two phases is crossed. AQIA measures the 45^{o} and 135^{o} diagonal changes of the gray level of each pixel, and then replaces the original gray level of each pixel by the maximum diagonal gray level gradient of that pixel. Thus, most object and background pixels are assigned relatively small gray level gradient values, and edges have higher values. A histogram of the maximum diagonal gradients can be thresholded with previously described methods. One peak should represent the edges, and another the non-edges. Fig. 10 shows the edge-detected image from the original image in Fig. 4.

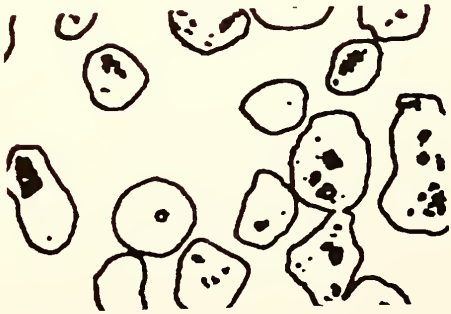

Figure 10

Edge-detected Image of Quartz

Generaly, edge-detection is used to detect the boundaries of objects. It might also be useful to detect thin-strip-type objects such as cracks. However, if the user wants to measure the objects, after edge-detection, the image needs to be filled.

BINARY IMAGE PROCESSING

Imperfect Binary Images and Some Processing Techniques

Occasionally, the binary image produced by segmentation is adequate for measurement. More often, the original image, or the sample itself, produces a binary image that is not yet ready for measurement. One problem may be that, because the original photograph has not been mounted in the digitizer properly, the area beyond the image of interest has also been digitized. If the resulting boundaries remains in the binary image, they will cause errors during measurement because the measuring procedures will treat them as objects. AQIA has a program called "trim" that can remove unwanted boundaries. This program asks the user to move the cursor to the desired upper left corner and the lower right corner. Then it produces a new binary image with the area outside of the points trimmed off. Fig. 9 is a binary image with such boundaries removed. Fig. 11 is the same binary image before trimming. The user should trim all binary images before measurements.

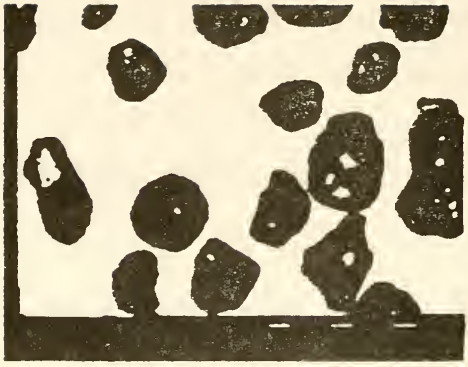

Figure 11

Binary Image before Trimming

Three more serious distortions or imperfections may also occur frequently. First, an image may have ´noise´ in the background phase that has the same gray level as the object phase. Second, some objects may be touching; therefore, they would be incorrectly treated as one object during measurement. Third, an object (or objects) may have some spots within that have the same gray level as the background phase due to reflected light. There are techniques to correct these distortions or imperfections in the binary image.

Imperfections in the original image photograph frequently produce spots in the background phase. This ´noise´ usually appears as small objects that are, in fact, artifacts. Frequently they can be filtered by a technique called erosion [17,36,37,39,40]. Erosion is similar to peeling an onion. The program searches for

points on objects' boundaries and changes these points' gray level to that of the background phase. A boundary point is defined as a point that has the same gray level as that of the object phase, and at least one neighbouring point having the gray level of the background phase. This process can be successively repeated with each step reducing the size of the objects by one boundary layer.

Both noise and the real objects of interest shrink during erosion, and they shrink from all sides. Usually the noise is smaller than the objects, therefore the noise will disappear first. If some objects are even smaller than the noise, these fine objects will become victims of this kind of noise filtering operation and will disappear also.

Touching objects can be separated by a series of erosion steps too[17,37,39,40]. When objects touch, the touching part is normally narrower than the bodies, so erosion can delete the touching part but retain the bodies. The objects, however, are reduced in size.

The complementary operation of erosion is called dilation. The program searches for points that have the gray level of the background phase, and at least one neighbouring point having the gray level of the object phase. Then it changes these points' gray level to that of the object phase. Dilation tends to recover the objects

that survive erosion. If an object has disappeared, it can not be dilated. Therefore, a series of dilation steps can be used to recover the surviving objects after filtering noise. But, if some fine objects have disappeared along with the noise, they can not be restored.

A series of dilation steps can also be used to recover surviving objects after separation when they were previously touching. But dilation must be stopped before these objects touch again. In other words, at least one row of background points must remain between two previously touching objects. If the objects touch at more than one place, the regions of contact may be of different sizes. Then there must be several rows of background points left between these objects. This will produce erroneous measurements because the objects aren't the original size.

In spot removal or filling, the program searches for points with the background's gray level that lie completely within an object. These are spot points. It then changes these points' gray level to that of the object phase. Spot removal is the most difficult of these operations. It needs a procedure called individual object selection [36].

In this process, the program searches for and records the first encountered boundary point. This is the point

to start. Then it searches for and records the next boundary point that is the nearest neighbour of the previous one. This process will be successively repeated to trace the boundary of the first encountered object. The tracing will stop when the starting point is encountered again. Finally, the area within the boundary will be filled to create the object. Before tracing the boundary of the next object, the previous one must be temporarily ´erased´ by treating it as the background. Obviously, this individual object selection can be used to fill spots. However, legitimate holes will be filled too.

From the above introduction of the currently and widely used image processing operations, it is evident that they have two shortcomings. They operate on all objects simultaneously, and they only can distinguish objects from the background phase by different gray levels, They can´t distinguish individual objects from each other. Therefore, some objects may be unnecessarily processed. In some cases, the processing will lead to erroneous measurements. Also, it will consume more processing time.

The root cause of these disadvantages is that typical operations can´t distinguish individual objects from each other. If individual objects could be identified, then filling or erosion could be performed only on selected objects which need to be filled, filtered or separated. If

individual objects could be distinguished from each other by some criteria other than gray level, then the eroded objects could be dilated all the way back to the point where they touch again. Re-touching would not make them indistinct. Techniques for individual selection have been developed. AQIA adapts a process called object labeling to label individual objects so that they can be distinguished easily from each other by different labels, and therefore correctly selected. Object labeling makes the binary image processing more precise and safer. Therefore, it makes image measurement more accurate and easier. It also allows measurements to be performed on each object in the image.

Individual Selection and Object Labeling

AQIA adapts object labeling to distinguish individuals from each other. The basic algorithm is given in reference [38]. That algorithm is improved in AQIA to label each feature in either the object phase or the background phase. Features with the background gray level could be legitimate holes in donut-like objects. The algorithm assumes pixels have 4-connectedness. This means that each pixel has four neighbours: north, south, west and east of it. Three row-by-row scans are performed on the image. The scans are performed from west to east with

the northern most row being looked at first and the process continuing to the south. Each point only needs to be compared to its north and west neighbours, which will have already been scanned and labeled.

During the first scan, if a point has a different gray level from both of its north and west neighbours, it will be assigned a new label. If it has the same gray level as that of its north neighbour but different from that of its west neighbour, it will be assigned the same label as that of its north neighbour. If it has the same gray level as that of its west neighbour but different from that of its north neighbour, it will be assigned the same label as that of its west neighbour. If it has the same gray level as both of its north and west neighbours, it will be assigned the same label as that of its west neighbour, and the equivalence between the labels of its north and west neighbours will be recorded. This forms an equivalence pair.

When this scan is complete, every point has a label, but different labels may have been assigned to points in the same feature. The program then finds the equivalences between the equivalence pairs indicating points in the same feature, and puts them together in one class. This results in a set of equivalence classes, each class containing all the labels which have been assigned to the same feature. AQIA uses integers as labels. The program

selects the smallest label in each equivalence class as the representative label of that class.

During the second scan, each label will be replaced by the representative label of its class. After the second scan, each feature in either phase has a unique integer as its label, but these integers may not form a continuous series. The program will then 'compress' the integer set to make these integers continuous. The third scan will re-label the features using continuous integers. After labeling, the binary image processing and measurement become very straightforward.

Overall and Individual Processing Modes

After features are uniquely labeled, noise filtering, object separation and spot filling can be performed in two modes: overall processing and individual processing. The algorithms of either mode become much easier after labeling. The labeled features could be real objects of interest, real spots to be filled, legitimate holes to be retained, etc.

For the individual mode of all these three operations, an individual feature must be selected first as follows. AQIA uses a Tektronix graphics monitor. The monitor allows one to move the cursor to any point on an

image displayed on the screen. Then the coordinates of that point will be automatically determined. Once the coordinates of a point are determined, the point's label can be found. If any point in a specified feature is located, all the points with the label of the specified feature can be found and the feature of interest is identified.

If there are no donut-like objects, the overall mode can be selected for filling spots. The program searches for points that have the labels different from that of the background, but the same gray level as that of the background. Then it changes their labels and gray level to those of the surrounding object. Fig. 12 is an example of the overall filling of the binary image in Fig. 9.

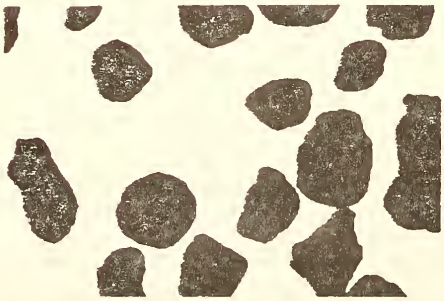

Figure 12

Overall Mode of Spot Filling

If there are some donut-like objects, the individual mode must be selected to fill only spots and to save real holes

in donut-like objects. First, a spot is selected with the cursor, and its label is found. Then the program searches for points having the label of the selected spot. It changes their label and gray level to those of the surrounding object. Legitimate holes won't be affected, since they are not selected with the cursor. If, in Fig. 9, only the bigger object on the left has a spot to be filled, then Fig. 13 shows the image after this individual filling.

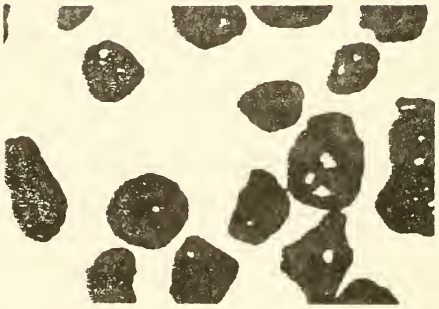

Figure 13

Individual Mode of Spot Filling

The user must remember that once the overall mode has been called, the individual mode won't be useful any more. Therefore, the user should be careful when calling the overall mode. On the other hand, sometimes, the spots might be too small to be recognized on the screen. If the user calls the individual mode, these tiny spots may be missed. However, the overall mode will find and fill

them. Therefore, it may be wise to ask for overall spot filling even when an image without legitimate holes appears to have no spots in its objects.

If there are no objects smaller than some noise that may be present, the overall mode can be selected for filtering the noise. The filtering is done by a sufficient number of erosion steps. Assume that the object in the upper left corner of Fig. 12 is noise. Fig. 14 shows the image filtered by overall erosion until this object is gone.

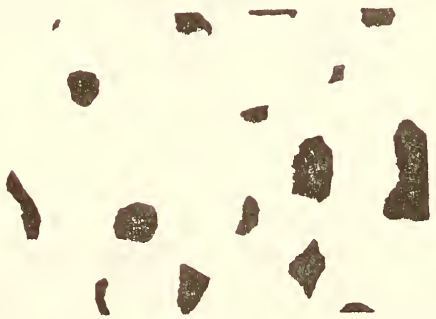

Figure 14

Overall Mode of Erosion for Noise Filtering

If there are objects smaller than the noise, the individual mode must be selected to filter only the real noise and retain the fine objects of interest. First, the noise is located with the cursor, and its label is found. The program erodes only the selected noise. The fine objects of interest won't be disturbed. Fig. 15 is copied from

Fig. 12, and one object is assumed to be a noise. Fig. 16 shows the image with that noise filtered by this individual erosion process.

Figure 15

An Image with Noise

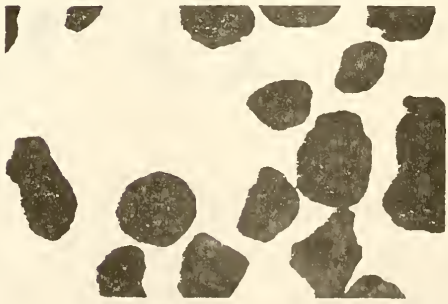

Figure 16

Individual Mode of Erosion for Noise Filtering

If no fine objects of interest will be deleted during erosion, the overall mode may be selected for separation of touching objects. The program erodes all the objects until the touching ones are separated. Fig. 17 shows the overall erosion of the filled image in Fig. 12, with the three touching objects separated.

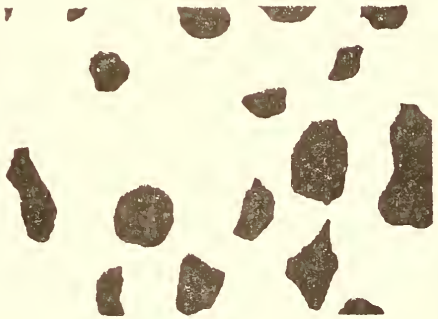

Figure 17

Overall Mode of Erosion for Object Separation

In the individual mode of separation, first, the touching objects are selected and their label is found. The touching aggregation has only one label. Then the program only erodes this label until separation. Fig. 18 shows individual erosion with the three touching objects separated and the other objects untouched.

The processes of noise filtering and object separation have left some objects in Fig. 14, 17 and 18 in a shrunken state. These must be dilated before they are

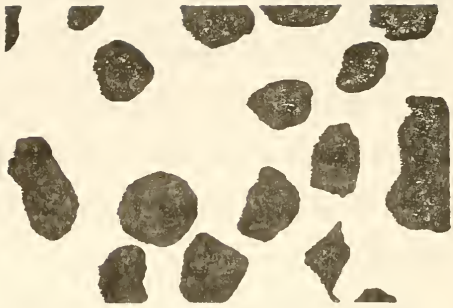

Figure 18

Individual Mode of Erosion for Object Separation

measured. After separation, the eroded image needs to be re-labeled so that the previously touching objects will have different labels. Then dilation may restore them until the previously touching objects touch again. Fig. 19 shows part of a labeled image with two objects touching and both being labeled 8. Fig. 20 shows the re-labeled image after separation and restoration, where these two objects now are labeled 8 and 9 respectively. They still touch, but now they can be distinguished by the different labels.

A difference between overall and individual erosion is that the depth of erosion and dilation is the same for all objects in the overall mode, while in the individual mode, the depth of erosion and dilation may be different for different objects, depending on the size of the touching regions. A bigger touching region will need more

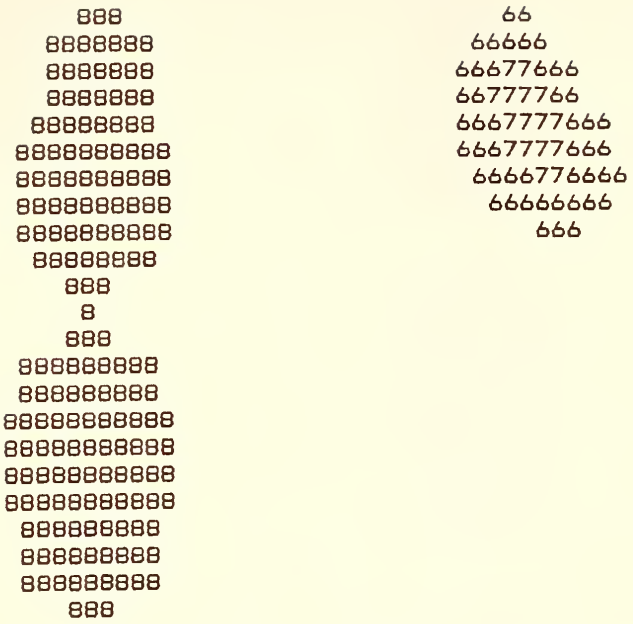

Figure 19

Part of a Labeled Image

erosion steps to separate the bodies, and therefore more dilation steps to recover the bodies. Therefore, the individual mode allows the surviving objects (bodies) to be recovered as precisely as possible.

If an object has some narrow ´peninsulas´, these narrow parts might not be able to survive the erosion necessary to separate a touching region. Therefore, the recovered objects might be the ´continent´ with the ´peninsulas´ removed. This is a common shortcoming of any

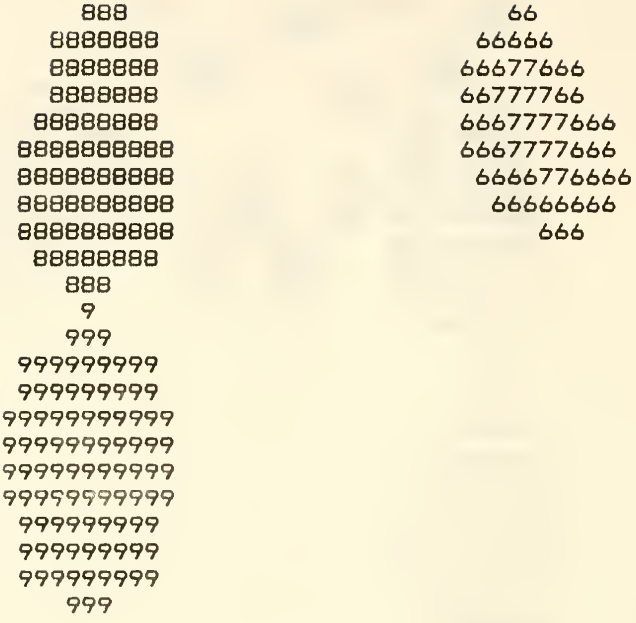

Figure 20

Part of a Re-labeled Image after Separation

dilation-type recovery. What labeling can contribute is to recover the 'continent' as completely as possible.

In practice, some combination of these two modes may be applied. For example, if there are some aggregations of touching objects, it may be more effective to first use the overall mode to 'thin' the touching parts. Then the individual mode can completely separate the remaining touching objects in each aggregation.

The adaptation of object labeling in AQIA can provide more precise and safer binary image processing than non-

labeling image analysis systems. Because the precision of image processing determines the reliability of the image measurement, AQIA is expected to provide more accurate and easier image measurement.

AQIA has two procedures called ´bitshow´ and ´erod.calc´. The first, ´bitshow´ asks the user to enter the lower and upper bounds from the gray level histogram or the fuzzy thresholding program. It then displays the thresholded image on the screen. It allows the user to change the bounds until he/she is satisfied with the binary image. If there are some spots to be filled, ´bitshow´ allows the user to choose either the overall or individual filling mode, or the individual followed by the overall mode. The image is labeled before either mode is called, because labeling makes the filling algorithm much easier. ´Bitshow´ will output the spot-free binary image.

If no more binary image processing is needed, the spot-free binary image can be measured by AQIA´s measuring procedures that include ´sep.calc´ for measuring the projections of separated particles, ´cut.calc´ for estimating 3-dimensional properties of microstructures from 2-dimensional measurements on the cut plane, and ´all.clac´ for both.

If erosion is needed, the procedure ´erod.calc´ must be called following ´bitshow´. It allows the user to

choose either the overall or individual mode of erosion, or the overall followed by the individual mode. After erosion, the image will be re-labeled, and the appropriate dilation will be performed. After that, the measurements will be performed on the processed binary image. Within ´erod.calc´ the user will find measurement options similar to ´sep.calc´, ´cut.calc´ and ´all.calc´. ´Erod.calc´ will output the final results of the measurements and the binary image that is free of spots and noise.

No labeled image will be output by either ´bitshow´ or ´erod.calc´, because a labeled image requires a great deal more disk space for storage than does a binary image. ´Erod.calc´ combines some of the image processing with the measurements since this avoids the necessity of relabeling the image if a subsequent measuring program were to be called.

BINARY IMAGE MEASUREMENT

Global and Individual Measurement

There are two classes of image measurements that can be performed by many image analysis systems: global measurements and individual measurements [37]. The more important global measurements include the area fraction of intercepted objects by a test plane, A_A, and the number of intersections with the boundaries of objects by a test line, N_L. The algorithms for a global measurement are straightforward because no individual object selection is involved.

For measuring A_A, the program only needs to count the pixels with the gray level of the object phase, because the object phase has a different gray level from that of the background. The number of these pixels divided by the total number of pixels is the area fraction of the object phase, A_A.

For measuring N_L, a test line across an image may intercept object boundaries. A boundary point is charac-

terized by having at least one of its neighbourings that have a different label. The number of the boundary points on the test line is N_L. Note that using labels, instead of gray levels, to characterize the boundary points makes AQIA also applicable to boundary points where two objects touch.

A_A and N_L are properties of two dimensional images that are directly measurable. Three dimensional properties of microstructures such as the volume fraction of objects and the surface area of objects per unit bulk volume can be estimated from these two dimensional properties. The volume fraction of the objects, V_V, can be estimated by:

$$V_V = \overline{A_A} \tag{20}$$

where $\overline{A_A}$ is the mean value of A_A [1, 2, 13].

The surface area of the objects per unit bulk volume can be estimated by:

$$S_V = 2\ \overline{N_L} \tag{21}$$

where $\overline{N_L}$ is the mean value of N_L [1, 2, 41]. The spatial size distribution of objects can also be estimated from the distribution of intercepted chord lengths and will be discussed later.

Object counting is an easy process for manual exami-

nation, but, without labeling, one of the most difficult processes in automatic image analysis. In AQIA, because the objects are separately labeled by integers, the total number of objects becomes the immediate result of the labeling process. This is an advantage of AQIA over image analysis systems without a labeling facility.

The measurements of individual objects include the perimeters, areas, and dimensions of these objects. After individual objects are uniquely labeled, the perimeter of a specific object is the number of boundary points with that object's label. The area of a specific object is the total number of points with that object's label. The dimension can be expressed by the maximum chord length of the specified object in some direction. Labeling makes individual measurements as straightforward as global ones. AQIA not only measures the perimeters, areas, maximum north-south and west-east chord lengths of all individual objects, but also calculates the means, maximums, minimums and distributions of these parameters.

Estimation of Spatial Size Distribution

The extrapolation from two to three dimensional space can give estimations of the volume fraction, surface area of objects per unit bulk volume, and the spatial size distribution of objects. For the former two estimations, the

only assumption needed is the randomness of the objects' distribution. For the estimation of size distribution, conventional methods need one more assumption: the objects must be spherical [1, 2, 42]. This must be assumed even if it is known that the objects are not spheres. Among these methods, Spektor's method is very simple [42]: In this method, the distances between pairs of boundary points that are on a test line, and have the same label, are defined as intercepted chord lengths. If the intercepted chord lengths are grouped into i groups, where i = 1, 2, ... with chord length increment Δ between groups, the spatial size distribution can be estimated by:

$$N_V(i) = \frac{4}{\pi\Delta^2}\left|\frac{N_L(i)}{2i - 1} - \frac{N_L(i+1)}{2i + 1}\right| \qquad (22)$$

where $N_V(i)$ is the number of particles (per unit bulk volume) with diameter in the interval $i\Delta - \Delta/2$ to $i\Delta + \Delta/2$. $N_L(i)$ and $N_L(i+1)$ are the number of intercepted chords per unit length of a test line in ith and (i + 1)th classes respectively.

AQIA uses Spektor's method to estimate the spatial size distribution of particles. Procedures 'cut.calc', 'all.calc' and 'erod.calc' ask the user to enter the chord length increment, Δ, and calculate the size distribution, $N_V(i)$. However, the assumption that the particles are spherical is a severe restriction for most real applications. Also, this method has a tendency to pick up a

false number of small chords, especially from particles having less regular shape [1,42]. AQIA has available a different approach to attack this problem. With this different approach, it can estimate the spatial size distribution of objects of any given shape, as long as the shape can be modeled. The algorithm is as follows.

The following factors are first defined. $p(V_i)$ is the relative frequency of objects of volume V_i with respect to total number of objects in three dimensional space. $p(x)$ is the relative frequency of intercepted chords with length x with respect to the total number of intercepted chords. $p(x|V_i)$ is the conditional probability (See Appendix A) that an intercepted chord with length x is from an object of volume V_i. Each chord of length x could be from any object that has a maximum dimension greater than x. According to the concepts of conditional probability [43], we can have (See Appendix A, Eqn. A.6 - A.8):

$$p(x) = \Sigma\ p(x|V_i)\ p(V_i) \tag{23}$$

where $p(V_i)$ is to be estimated; and $p(x)$ is obtained from measurements on cut planes through the volume. If there are n classes of the intercepted chords, Eqn. 23 will expand into n linear simultaneous equations. If all the $p(x|V_i)$ can be obtained in some way, all the $p(V_i)$ can be calculated by solving the linear equations.

AQIA uses computer simulation to obtain $p(x|V_i)$. We define $p(x)$ as the distribution of all measured chord lengths, and $p(x|V_i)$ as the distribution of simulated chord lengths from objects of volume V_i. Consider a particle of volume V_i and with a surface defined by $f(x,y,z) = 0$, and having maximum dimension $d_{max,i}$. Assuming the function $f(x,y,z) = 0$ can be modeled, a pair of points, (x1,y1,z1) and (x2,y2,z2), can be picked randomly on the surface $f(x,y,z) = 0$. (The two points can't be on the same plane surface because a line between them does not intercept the particle.) The distance between these two points is the length of an intercepted chord.

A sufficient number of chords, collected randomly with a computer program, will result in a distribution of simulated chord lengths, $p(x|V_i)$ vs. x, where x ranges from 0 to the maximum dimension, $d_{max,i}$. The ratio $x/d_{max,i}$ instead of x is used as the independent variable so that the range of the independent variable, $x/d_{max,i}$, is from 0 to 1. Thus, the value of V_i or $d_{max,i}$ alone doesn't affect the results. Only the ratio of the randomly intercepted chord length to the maximum chord, $x/d_{max,i}$, determines the distribution of simulated chord lengths. In other words, for any volume V, the distribution of simulated chord lengths could be expressed as:

$$p(x|V) = p(\frac{x}{d_{max}}) \qquad (24)$$

The subscript i is omitted, because the equation holds for any volume. In references [44-46], this computer simulation method was used to model the chord length distribution of particles of the same size.

After the simulated chord length distribution, $p(x|V_i)$ is obtained by a computer program, and the measured chord length distribution, $p(x)$, is measured, all the $p(V_i)$ can be calculated by solving the linear equations in Eqn. 23. If the number of classes into which the volumes of objects are desired to be grouped is chosen to be n, in order to obtain finite solutions for n linear equations, the measured chord lengths must also be grouped into n classes, and the following relation must hold:

$$\frac{x_i}{d_{max,i}} \leq 1 \qquad (25)$$

where x_i is the measured chord length of ith class, and $d_{max,i}$ is the maximum dimension of objects in ith class. Obviously, if $x_i/d_{max,i} > 1$, then $p(x/d_{max,i}) = 0$, and no solution exists for $p(V_i)$.

Suppose n is selected as 3. The measured chord lengths should also be grouped into 3 classes. We have 3 linear equations:

$$\begin{aligned} p(x_1) &= p(x_1|V_1)p(V_1)+p(x_1|V_2)p(V_2)+p(x_1|V_3)p(V_3) \qquad (26)\\ p(x_2) &= p(x_2|V_1)p(V_1)+p(x_2|V_2)p(V_2)+p(x_2|V_3)p(V_3)\\ p(x_3) &= p(x_3|V_1)p(V_1)+p(x_3|V_2)p(V_2)+p(x_3|V_3)p(V_3) \end{aligned}$$

Because of Eqn. 24, the linear equations can be rewritten as:

$$p(x_1) = p(\frac{x_1}{d_{max,1}})p(V_1)+p(\frac{x_1}{d_{max,2}})p(V_2)+p(\frac{x_1}{d_{max,3}})p(V_3) \quad (27)$$

$$p(x_2) = p(\frac{x_2}{d_{max,1}})p(V_1)+p(\frac{x_2}{d_{max,2}})p(V_2)+p(\frac{x_2}{d_{max,3}})p(V_3)$$

$$p(x_3) = p(\frac{x_3}{d_{max,1}})p(V_1)+p(\frac{x_3}{d_{max,2}})p(V_2)+p(\frac{x_3}{d_{max,3}})p(V_3)$$

All $p(x_i)$ are obtained from the actual measurements on cut surface of the system, and all $p(x_i/d_{max,j})$ are obtained from the computer simulation. With these, we can solve for all $p(V_i)$.

The conventional methods require that the particles be spherical, no matter that the shape is known or unknown. The AQIA method does not require a particular shape. As long as the shape is known and can be modeled, this method is applicable. In real applications, the shape is sometimes unknown. A database could be developed that would contain the distributions of simulated chord lengths, $p(x|V_i)$, of many modelable shapes. Then a software system could be used that would allow the user to assume a shape, then find the corresponding $p(x|V_i)$ from the database, and check the shape assumption.

The checking algorithm would be as follows. The specific surface area per unit particle volume can be estimated in two ways. First, it equals the surface area

of the particles per unit bulk volume, S_V, divided by the volume fraction, V_V. The estimations of V_V and S_V need not to assume a shape, therefore, the measurement of the specific surface area based on V_V and S_V is independent of shape. This value of the specific surface area is called $S_{spe.1}$. Secondly, if the shape of the particles is assumed, and the size distribution is obtained, then the specific surface area can also be obtained based on the size distribution and the assumed shape. This value of the specific surface is called $S_{spe.2}$. If $S_{spe.2}$ is close enough to $S_{spe.1}$, the shape assumption may be considered valid. If $S_{spe.2}$ is not close to $S_{spe.1}$, another shape can be tried. The values of the specific surface areas from two different shape assumptions might be equally close to $S_{spe.1}$. But, increasing the number of the classes will show a tendency that only the $S_{spe.2}$ of the 'right' shape will approach $S_{spe.1}$ while that of another shape will deviate from $S_{spe.1}$.

A software system along this line could be developed. It would allow the user to change the shape assumption until the user is satisfied. This system would estimate both the size distribution and the shape of the particles. This development is beyond the scope of the present work. Thus, it is presently only implemented for spherical particles.

In AQIA, there is a program called ´newpsd´ that uses this new method to estimate the particle size distribution. At present, it has only the distribution of simulated chord lengths, $p(x/d_{max})$, for spherical particles in its database. The distribution of measured chord lengths, p(x), is automatically collected from the outputs of the measuring procedures. `Newpsd´ will give the size distribution p(V).

DEMONSTRATION AND VERIFICATION OF AQIA

Typical Results of Measurement on Separate Particles

Fig. 4 shows a projection of several particles of quartz. As Fig. 9 shows, its binary image is a good representation of the original image. Thus, it is ready to be processed and measured with AQIA. Figures 21 and 22 show the left part and the right part of the Fig. 9. These images will be used to demonstrate the typical results of using AQIA to measure separate particles.

Figure 21

Left Part of Fig. 9

Figure 22

Right Part of Fig. 9

These two parts are labeled Sample 1 and Sample 2 of Quartz. After using the ´bitshow´ program, the ´erod.calc´ program is needed to separate the touching particles. Then, each part was measured using the separate particle option of ´erod.calc´. Since these two parts are from the same material, the mean values of the measurements from separate images were also calculated by ´erod.calc´. The length unit that is used in all the results was entered by the user when the ´dscrb´ program was called. The typical, numeric results that are direct outputs from the ´erod.calc´ program, are shown in Tables 4 to 8. In these tables, the notation "x en" means that the value is multiplied by 10^n.

Table 4 shows the basic individual measurements that include perimeters, areas, and maximum chords in orthogonal directions. ("Extent" means maximum chord). Note that label 1 has been assigned to the background so that there

is no object labeled 1 listed in the table. Table 4 also gives the size (area) of the whole image, the area fraction of objects (intersections), the total number of objects, the number of objects per unit image area, and the maximum, minimum and mean values of the individual measurements. Sample 1 was processed first. Therefore, the mean values given in parentheses are the same as the Sample 1 values. When Sample 2 was processed next, the values in the parentheses were updated to reflect the means of both samples.

Table 5 shows the distribution of the perimeters. The number frequency, the relative frequency and the cumulative frequency are included. The interval between classes is 300 microns. Taking the data for the 4th interval as an example, the results show that, in Sample 1, there are 2 particles, or 25% of the total particles that have perimeters between 90 and 120 microns, and that 50% of the total particles have the perimeters less than 120 microns. The data for the 4th interval for Sample 2 show that the average number of particles in the two images, with perimeters between 90 and 120 microns, is 1.5, the average percentage of particles with perimeters between 90 and 120 microns is 17.05%, and the average percentage of particles with perimeters less than 120 microns is 43.18%. Note that the number of classes in Sample 2 is greater than that in Sample 1 because the biggest perime-

ter in Sample 2 is greater than that in Sample 1.

Tables 6 to 8 show the distributions of maximum chords and areas. Again, the number frequency, the relative frequency and the cumulative frequency are included. The structure of these tables is similar to Table 4. In the distribution of west-east maximum chords, the interval between classes is 50 microns. In the distribution of north-south maximum chords, the interval is 100 microns. In the distribution of areas, the interval is 4×10^4 square microns.

Table 4

Basic Measurements on Quartz

Sample 1 of Quartz

The length unit is microns
In the () is the mean value for all the samples above.

Image size (x e8):		0.0355
Area fraction of intersections:		0.3057
	(	0.3057)
Total Number of intersections:		8
# of intersection/unit area (x e-8):		225.51
	(	225.51)
Max. perimeter of intersections (x e4):		0.1860
Min. perimeter of intersections:		0.0670
Mean perimeter of intersections:		0.1220
	(	0.1220)
Maximun area of intersections (x e8):		0.0026
Minimun area of intersections:		0.0003
Mean area of intersections:		0.0014
	(	0.0014)
Max.w-e extent of intersections (x e4):		0.0590
Min.w-e extent of intersections:		0.0110
Mean w-e extent of intersections:		0.0371
	(	0.0371)
Max.n-s extent of intersections (x e4):		0.0770
Min.n-s extent of intersections:		0.0180
Mean n-s extent of intersections:		0.0426
	(	0.0426)

Labels				
Perimeter				
Area	W-E Extent		N-S Extent	
	(x e4)	(x e8)	(x e4)	(x e4)
0	0.0750	0.0003	0.0110	0.0330
2	0.0670	0.0004	0.0250	0.0180
3	0.1160	0.0010	0.0380	0.0320
4	0.1240	0.0016	0.0450	0.0480
5	0.1860	0.0026	0.0420	0.0770
6	0.1600	0.0026	0.0590	0.0570
7	0.1360	0.0014	0.0410	0.0420
8	0.1120	0.0010	0.0360	0.0340

Table 4 (continued)

Sample 2 of Quartz

The length unit is microns
In the () is the mean value for all the samples above.

Image size (x e8):	0.0355
Area fraction of intersections:	0.4798
	(0.3927)
Total Number of intersections:	11
# of intersection/unit area (x e-8):	309.56
	(267.54)
Max. perimeter of intersections (x e4):	0.2580
Min. perimeter of intersections:	0.0680
Mean perimeter of intersections:	0.1328
	(0.1274)
Maximun area of intersections (x e8):	0.0041
Minimun area of intersections:	0.0002
Mean area of intersections:	0.0015
	(0.0015)
Max.w-e extent of intersections (x e4):	0.0600
Min.w-e extent of intersections:	0.0120
Mean w-e extent of intersections:	0.0425
	(0.0398)
Max.n-s extent of intersections (x e4):	0.1020
Min.n-s extent of intersections:	0.0130
Mean n-s extent of intersections:	0.0448
	(0.0437)

Labels				
Perimeter				
Area	W-E Extent		N-S Extent	
	(x e4)	(x e8)	(x e4)	(x e4)
0	0.0730	0.0004	0.0180	0.0280
2	0.1240	0.0008	0.0600	0.0160
3	0.1300	0.0011	0.0510	0.0270
4	0.1140	0.0012	0.0360	0.0380
5	0.1200	0.0014	0.0470	0.0390
6	0.2580	0.0041	0.0510	0.1020
7	0.1910	0.0034	0.0580	0.0740
8	0.1410	0.0017	0.0410	0.0570
9	0.1610	0.0023	0.0540	0.0660
10	0.0680	0.0002	0.0120	0.0330
11	0.0810	0.0004	0.0400	0.0130

Table 5

Distribution of Perimeters of Quartz

The length unit is microns.
In the () are the mean values for all the samples above.

Sample #	Start-with (x e4)	Frequency	Rel.Freq.	Cum.Freq.
1	0.000	0	0.0000	0.0000
		(0)	(0.0000)	(0.0000)
1	0.030	0	0.0000	0.0000
		(0)	(0.0000)	(0.0000)
1	0.060	2	0.2500	0.2500
		(2)	(0.2500)	(0.2500)
1	0.090	2	0.2500	0.5000
		(2)	(0.2500)	(0.5000)
1	0.120	2	0.2500	0.7500
		(2)	(0.2500)	(0.7500)
1	0.150	1	0.1250	0.8750
		(1)	(0.1250)	(0.8750)
1	0.180	1	0.1250	1.0000
		(1)	(0.1250)	(1.0000)
2	0.000	0	0.0000	0.0000
		(0.0000)	(0.0000)	(0.0000)
2	0.030	0	0.0000	0.0000
		(0.0000)	(0.0000)	(0.0000)
2	0.060	3	0.2727	0.2727
		(2.5000)	(0.2614)	(0.2614)
2	0.090	1	0.0909	0.3636
		(1.5000)	(0.1705)	(0.4318)
2	0.120	4	0.3636	0.7273
		(3.0000)	(0.3068)	(0.7386)
2	0.150	1	0.0909	0.8182
		(1.0000)	(0.1080)	(0.8466)
2	0.180	1	0.0909	0.9091
		(1.0000)	(0.1080)	(0.9545)
2	0.210	0	0.0000	0.9091
		(0.0000)	(0.0000)	(0.9545)
2	0.240	1	0.0909	1.0000
		(0.5000)	(0.0455)	(1.0000)

Table 6

Distribution of Max. W-E Chords of Quartz

The length unit is microns.
In the () are the mean values for all the samples above.

Sample #	Start-with (x e4)	Frequency	Rel.Freq.	Cum.Freq.
1	0.000	0	0.0000	0.0000
		(0)	(0.0000)	(0.0000)
1	0.005	0	0.0000	0.0000
		(0)	(0.0000)	(0.0000)
1	0.010	1	0.1250	0.1250
		(1)	(0.1250)	(0.1250)
1	0.015	0	0.0000	0.1250
		(0)	(0.0000)	(0.1250)
1	0.020	0	0.0000	0.1250
		(0)	(0.0000)	(0.1250)
1	0.025	1	0.1250	0.2500
		(1)	(0.1250)	(0.2500)
1	0.030	0	0.0000	0.2500
		(0)	(0.0000)	(0.2500)
1	0.035	2	0.2500	0.5000
		(2)	(0.2500)	(0.5000)
1	0.040	2	0.2500	0.7500
		(2)	(0.2500)	(0.7500)
1	0.045	1	0.1250	0.8750
		(1)	(0.1250)	(0.8750)
1	0.050	0	0.0000	0.8750
		(0)	(0.0000)	(0.8750)
1	0.055	1	0.1250	1.0000
		(1)	(0.1250)	(1.0000)

Table 6 (continued)

Sample #	Start-with (x e4)	Frequency	Rel.Freq.	Cum.Freq.
2	0.000	0	0.0000	0.0000
		(0.0000)	(0.0000)	(0.0000)
2	0.005	0	0.0000	0.0000
		(0.0000)	(0.0000)	(0.0000)
2	0.010	1	0.0909	0.0909
		(1.0000)	(0.1080)	(0.1080)
2	0.015	1	0.0909	0.1818
		(0.5000)	(0.0455)	(0.1534)
2	0.020	0	0.0000	0.1818
		(0.0000)	(0.0000)	(0.1534)
2	0.025	0	0.0000	0.1818
		(0.5000)	(0.0625)	(0.2159)
2	0.030	0	0.0000	0.1818
		(0.0000)	(0.0000)	(0.2159)
2	0.035	1	0.0909	0.2727
		(1.5000)	(0.1705)	(0.3864)
2	0.040	2	0.1818	0.4545
		(2.0000)	(0.2159)	(0.6023)
2	0.045	1	0.0909	0.5455
		(1.0000)	(0.1080)	(0.7102)
2	0.050	3	0.2727	0.8182
		(1.5000)	(0.1364)	(0.8466)
2	0.055	1	0.0909	0.9091
		(1.0000)	(0.1080)	(0.9545)
2	0.060	1	0.0909	1.0000
		(0.5000)	(0.0455)	(1.0000)

Table 7

Distribution of Max. N-S Chords of Quartz

The length unit is microns.
In the () are the mean values for all the samples above.

Sample #	Start-with (x e4)	Frequency	Rel.Freq.	Cum.Freq.
1	0.000	0	0.0000	0.0000
		(0)	(0.0000)	(0.0000)
1	0.010	1	0.1250	0.1250
		(1)	(0.1250)	(0.1250)
1	0.020	0	0.0000	0.1250
		(0)	(0.0000)	(0.1250)
1	0.030	3	0.3750	0.5000
		(3)	(0.3750)	(0.5000)
1	0.040	2	0.2500	0.7500
		(2)	(0.2500)	(0.7500)
1	0.050	1	0.1250	0.8750
		(1)	(0.1250)	(0.8750)
1	0.060	0	0.0000	0.8750
		(0)	(0.0000)	(0.8750)
1	0.070	1	0.1250	1.0000
		(1)	(0.1250)	(1.0000)
2	0.000	0	0.0000	0.0000
		(0.0000)	(0.0000)	(0.0000)
2	0.010	2	0.1818	0.1818
		(1.5000)	(0.1534)	(0.1534)
2	0.020	2	0.1818	0.3636
		(1.0000)	(0.0909)	(0.2443)
2	0.030	3	0.2727	0.6364
		(3.0000)	(0.3239)	(0.5682)
2	0.040	0	0.0000	0.6364
		(1.0000)	(0.1250)	(0.6932)
2	0.050	1	0.0909	0.7273
		(1.0000)	(0.1080)	(0.8011)
2	0.060	1	0.0909	0.8182
		(0.5000)	(0.0455)	(0.8466)
2	0.070	1	0.0909	0.9091
		(1.0000)	(0.1080)	(0.9545)
2	0.080	0	0.0000	0.9091
		(0.0000)	(0.0000)	(0.9545)
2	0.090	0	0.0000	0.9091
		(0.0000)	(0.0000)	(0.9545)
2	0.100	1	0.0909	1.0000
		(0.5000)	(0.0455)	(1.0000)

Table 8

Distribution of Areas of Quartz

The length unit is microns.
In the () are the mean values for all the samples above.

Sample #	Start-with (x e6)	Frequency	Rel.Freq.	Cum.Freq.
1	0.000	2	0.2500	0.2500
		(2)	(0.2500)	(0.2500)
1	0.040	0	0.0000	0.2500
		(0)	(0.0000)	(0.2500)
1	0.080	2	0.2500	0.5000
		(2)	(0.2500)	(0.5000)
1	0.120	2	0.2500	0.7500
		(2)	(0.2500)	(0.7500)
1	0.160	0	0.0000	0.7500
		(0)	(0.0000)	(0.7500)
1	0.200	0	0.0000	0.7500
		(0)	(0.0000)	(0.7500)
1	0.240	2	0.2500	1.0000
		(2)	(0.2500)	(1.0000)
2	0.000	3	0.2727	0.2727
		(2.5000)	(0.2614)	(0.2614)
2	0.040	1	0.0909	0.3636
		(0.5000)	(0.0455)	(0.3068)
2	0.080	2	0.1818	0.5455
		(2.0000)	(0.2159)	(0.5227)
2	0.120	1	0.0909	0.6364
		(1.5000)	(0.1705)	(0.6932)
2	0.160	1	0.0909	0.7273
		(0.5000)	(0.0455)	(0.7386)
2	0.200	1	0.0909	0.8182
		(0.5000)	(0.0455)	(0.7841)
2	0.240	0	0.0000	0.8182
		(1.0000)	(0.1250)	(0.9091)
2	0.280	0	0.0000	0.8182
		(0.0000)	(0.0000)	(0.9091)
2	0.320	1	0.0909	0.9091
		(0.5000)	(0.0455)	(0.9545)
2	0.360	0	0.0000	0.9091
		(0.0000)	(0.0000)	(0.9545)
2	0.400	1	0.0909	1.0000
		(0.5000)	(0.0455)	(1.0000)

Typical Results of Estimation on 3-Dimensional Properties

If Fig. 4 were a cut plane through a solid sample, the results in Tables 4 to 8 could be used to obtain estimates of the properties of the solid. In what follows, it will be assumed that Fig. 4 is such a cut plane. This ruse is used to circumvent the need for preparing a special sample merely to demonstrate the AQIA package. The 3-dimensional properties that can be estimated by AQIA are shown in Tables 9 and 10. These two tables also show the length unit used in the estimations and the mean values from the two separate images.

Table 9 shows the volume fraction, the surface area of objects per unit bulk volume, and the specific surface area of objects per unit object volume (based on the former two values). The total number of objects per unit bulk volume is given and is calculated from the size distribution based on the conventional method. Table 9 also shows the mean diameter of the objects, assuming that the objects are spheres.

Table 10 shows the size distribution based on the conventional method. The number frequency, the relative frequency and the cumulative frequency are included. The interval between classes is 100 microns. The conventional method derives the size distribution from the distribution

Table 9

Volume Fraction and Surface Areas from Fig. 9

VFA is volume fraction.
SV is surface area per unit bulk volume.
SSA is specific surface area per unit object volume.
TN is the total number of particles per unit bulk volume.
MD is the mean diameter of particles
The length unit is microns
In the () are the mean values for all the samples above.

Sample #	VFA	SV(x e-4)	SSA(x e-4)	TN(x e-10)	MD(x e4)
1	0.3057	29.9366	97.9280	44.8639	0.0367
	(0.3057)	(29.9366)	(97.9280)	(44.8639)	(0.0367)
2	0.4798	46.2093	96.3094	116.1319	0.0278
	(0.3927)	(38.0729)	(97.1187)	(80.4979)	(0.0322)

of the intercepted chords of objects by a random test line. The mean lengths of the intercepted chords in each class are used as the mean diameters of objects in that class. Table 10 also includes the number frequency of intersected chords' lengths. For example, the data for the 4th interval for Sample 1 show that there are 109 intercepted chords with mean length 350 microns, or 8.6025×10^{-10} particles with mean diameter 350 microns per cubic micron bulk volume, and the percentage of particles with mean diameter 350 microns is 19.17%, the percentage of particles with diameter less than 400 microns is 56.89%.

The comparison between the conventional method and the new method for estimating the size distribution will be presented later.

Table 10

Particles Size Distribution from Fig.9

The length unit is microns. Chd stands for intersected chords.
In the () are the maen values for all the samples above.
Frequency is the number of particles per unit bulk volume.

Sample #	Ave.Dia. (x e4)	Freq.(x e-10)	Rel.freq.	Cum.Freq.	Chd.Freq.
1	0.0050	0.0000	0.0000	0.0000	25
		(0.0000)	(0.0000)	(0.0000)	(25)
1	0.0150	14.7153	0.3280	0.3280	75
		(14.7153)	(0.3280)	(0.3280)	(75)
1	0.0250	2.2047	0.0491	0.3771	84
		(2.2047)	(0.0491)	(0.3771)	(84)
1	0.0350	8.6025	0.1917	0.5689	109
		(8.6025)	(0.1917)	(0.5689)	(109)
1	0.0450	6.6163	0.1475	0.7164	97
		(6.6163)	(0.1475)	(0.7164)	(97)
1	0.0550	8.8598	0.1975	0.9138	78
		(8.8598)	(0.1975)	(0.9138)	(78)
1	0.0650	0.9939	0.0222	0.9360	28
		(0.9939)	(0.0222)	(0.9360)	(28)
1	0.0750	2.4490	0.0546	0.9906	24
		(2.4490)	(0.0546)	(0.9906)	(24)
1	0.0850	0.4222	0.0094	1.0000	4
		(0.4222)	(0.0094)	(1.0000)	(4)

Table 10 (continued)

Particles Size Distribution from Fig.9

Sample #	Ave.Dia. (x e4)	Freq.(x e-10)	Rel.freq.	Cum.Freq.	Chd.Freq.
2	0.0050	48.9697	0.4217	0.4217	55
		(24.4849)	(0.2108)	(0.2108)	(40.0000)
2	0.0150	1.1944	0.0103	0.4320	83
		(7.9548)	(0.1691)	(0.3800)	(79.0000)
2	0.0250	0.0000	0.0000	0.4320	135
		(1.1023)	(0.0246)	(0.4045)	(109.5000)
2	0.0350	41.5190	0.3575	0.7895	247
		(25.0608)	(0.2746)	(0.6792)	(178.0000)
2	0.0450	0.3619	0.0031	0.7926	109
		(3.4891)	(0.0753)	(0.7545)	(103.0000)
2	0.0550	19.2688	0.1659	0.9585	131
		(14.0643)	(0.1817)	(0.9362)	(104.5000)
2	0.0650	0.0000	0.0000	0.9585	15
		(0.4970)	(0.0111)	(0.9473)	(21.5000)
2	0.0750	2.3536	0.0203	0.9788	25
		(2.4013)	(0.0374)	(0.9847)	(24.5000)
2	0.0850	0.1609	0.0014	0.9802	6
		(0.2915)	(0.0054)	(0.9901)	(5.0000)
2	0.0950	0.0000	0.0000	0.9802	5
		(0.0000)	(0.0000)	(0.9901)	(2.5000)
2	0.1050	2.3035	0.0198	1.0000	27
		(1.1517)	(0.0099)	(1.0000)	(13.5000)

Verification of Measurement on Separate Particles

Fig. 23 shows an image of 36 coins. Among these 36 coins there are 4 quarters, 6 nickles, 9 pennies and 17 dimes. The numbers of each coin were selected to give a reasonably uniform coin distribution in the space. These 36 coins were placed on a light table and photographed. The whole area taken in this image is 358mm x 278mm.

This image was divided into four parts of approximately equal areas. These four parts were digitized at a resolution that made one pixel approximately 0.41 mm. The four parts of the whole image were labeled Coin 1, Coin 2, Coin 3 and Coin 4 in the clockwise order from the upper right quadrant to the upper left one. Each part was measured using the `sep.calc´ program in AQIA. In addition, the mean values of the measurements from separate images were calculated to get the overall measurements that one would get if the entire image had been measured at once. These results were compared with the true values that could be calculated from the known sizes of the coins.

Image Coin 3 (the lower left part) will be used as an example of the process used on each of the four parts. Fig. 24 shows the original image of this part. Fig. 25 is the corresponding histogram of gray levels. Gray level 159 represents the population of the ´white´ coins. Using the peak gray levels 89 and 159 as two extremes, the

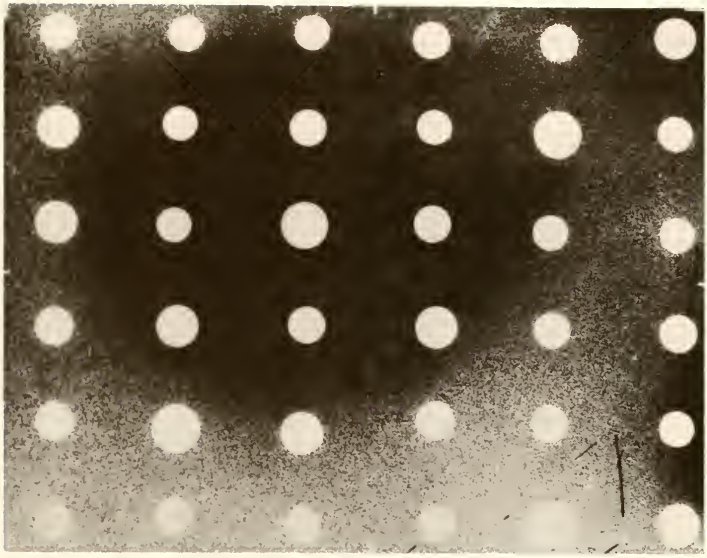

Figure 23

Original Image of Coins

´fuzzthr´ program suggested gray level 143 as the dividing level between these two extreme gray levels. Taking gray level 143 and 255 as the thresholding bounds results in Fig. 26 as the binary image.

The original image, Fig. 24 is not uniformly illuminated. This results in the confused histogram in Fig. 25. In cases such as this, some judgement must be exercised by the user in selecting extremes for the ´fuzzthr´ program. If other peaks that have gray levels less than 89 were used as the left extreme, the ´fuzzthr´ program would give a thresholding bound that would produce a binary image with obviously spurious objects in it.

Thus level 89 is the only lowest extreme that results in a sensible image.

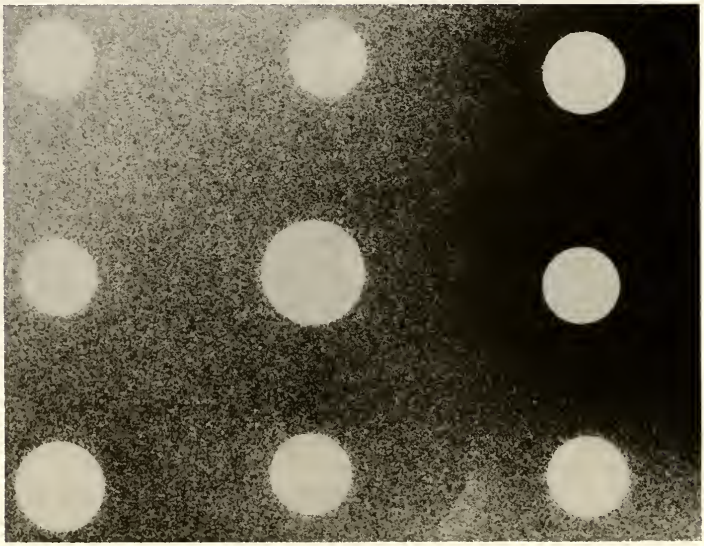

Figure 24

Original Image of Coin 3

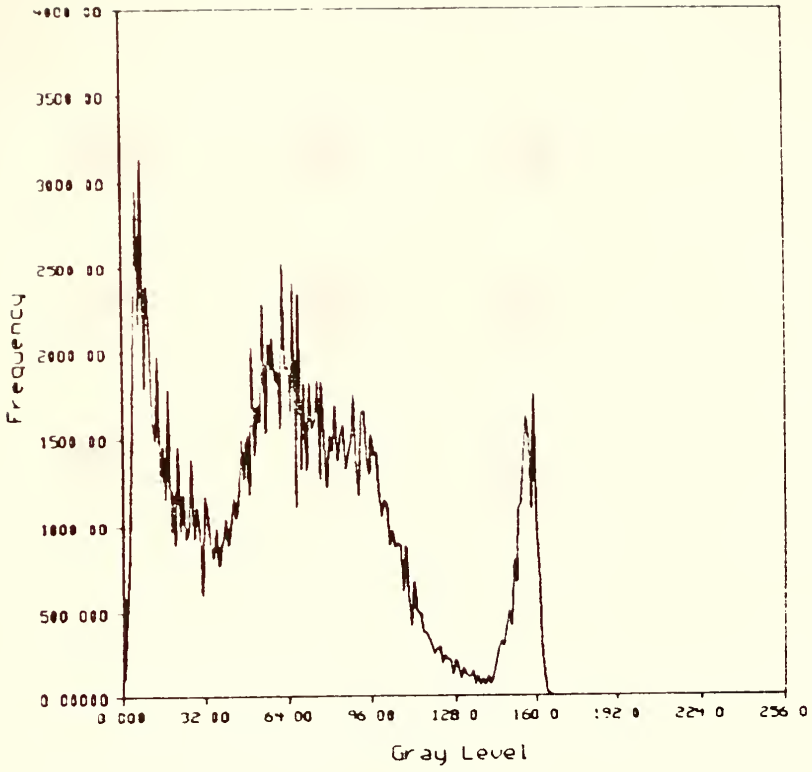

Figure 25

Histogram of Gray level (Coin 3)

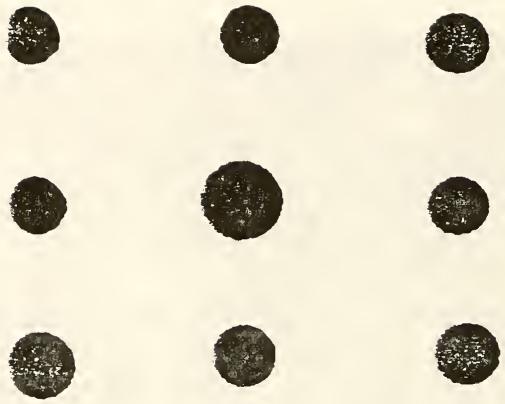

Figure 26

Binary Image of Coin 3

Table 11 shows the area fractions of each separate image and the mean area fraction that was calculated from these. These are compared with the true area factions that were directly calculated from coin and image sizes. The relative error between the mean area fraction of these four parts and the true value is satisfactorily low. This verifies both the validity of the new, fuzzy probability based method of image segmentation introduced in this work, and the accuracy of AQIA's area fraction measurement.

Table 11

Area Fractions of Coins

Images	AQIA Measurement %	True Value %	Rel. Error %
Coin 1	10.48	10.33	1.5
Coin 2	10.46	10.58	1.1
Coin 3	11.34	11.13	1.9
Coin 4	11.73	11.79	0.5
Mean of Combined	11.00	10.96	0.4

Tables 12 to 15 show the results of measurements on individual coins. All the measurements are the mean values from the 4 separate images. The accuracy of individual measurements is more dependent on the resolution of the digitizer and how the relevant pixels are counted. The resolution can always be improved, but high resolution

image needs more computation time.

Table 12 shows the perimeters of the different coins from AQIA measurements compared with the true values that were calculated. The AQIA measurements are all less than the true values and the relative errors are much higher than that of the area fractions. This is because, in the digitized image, a circle is represented by a polygon composed of pixels that are small squares. The side of one of these small squares is used as the length of one pixel. The centers of perimeter pixels must be near the coin's perimeter. Thus, the actual trace of a coin's perimeter through a square pixel will usually be greater than a pixel's edge. If the image were digitized at a higher resolution, the underestimation problem would be improved.

Table 12

Perimeters of Coins

Coins	AQIA measurement mm	True Value mm	Rel. error %
Quarter	70.08	75.40	7.1
Nickle	61.93	65.97	6.2
Dime	52.25	55.76	6.3
Penny	54.64	59.69	8.5

Table 13 shows the areas of the different coins from AQIA measurements compared with the true values. The AQIA values are all greater than the true ones. The centers of

border pixels must be near the true border of a coin. Thus, these on-border pixels have some area beyond the real border that is also counted when the areas are calculated. However, the relative errors are less than those for perimeters because on-border pixels are a smaller portion of total object pixels than they are of the perimeter. Again, this situation could be improved with a higher resolution.

Table 13

Areas of Coins

Coins	AQIA measurement mm^2	True Value mm^2	Rel. error %
Quarter	470.21	452.39	4.0
Nickle	364.14	346.36	4.9
Dime	252.56	247.45	2.1
Penny	292.77	283.53	3.3

Tables 14 and 15 show the maximum chords from AQIA measurements compared with the true values. The AQIA measurements are a little greater than the true values because each chord has two on-border pixels at its ends that slightly extend the chord. However, the relative errors are lower because the two on-border pixels are a small portion of the total chord pixels.

Tables 12 to 15 all show that the measurements on dimes have the least error because there were more dimes

Table 14

Max. W-E Chords of Coins

Coins	AQIA measurement mm	True Value mm	Rel. error %
Quarter	24.34	24.00	1.4
Nickle	21.93	21.00	4.4
Dime	17.88	17.75	0.73
Penny	19.29	19.00	1.5

Table 15

Max. N-S Chords of Coins

Coins	AQIA measurement mm	True Value mm	Rel. error %
Quarter	24.69	24.00	2.9
Nickle	21.40	21.00	1.9
Dime	17.93	17.75	1.0
Penny	19.23	19.00	1.2

in the images. This demonstrates the obvious point that increasing the number of objects of a type improves the accuracy of the individual measurements of that type.

Comparison of the Conventional Method and the New Method for Estimating the Particle Size Distribution

Fig. 27 shows a random part of the whole coin image that was taken from Fig. 23. Fig. 28 is the corresponding binary image segmented with the 'fuzzthr' program. This image was used to demonstrate the calculation of the particle size distribution of objects in a matrix by imagining that this image was a cut plane through a solid containing spherical inclusions. Calculations were made with the conventional method using the 'cut.calc' program and the new method using the 'newpsd' program. Fig. 29 shows the comparison between these two methods. This comparison was also made on the image Coin 3 and Fig. 30 shows the results.

Both methods find peaks roughly corresponding to the larger and smaller coins in the images. In addition, Fig. 29 has a peak at a small particle size that comes from the coins that were cut at the image boundaries. This emphasizes the importance of measuring enough objects so that edge effects are minimized.

As mentioned earlier, the conventional method has a tendency to calculate a false number of small chords. Figures 29 and 30 show this and that the new method does not have this tendency. Unfortunately, there is no true value of the size distribution available for verification. It

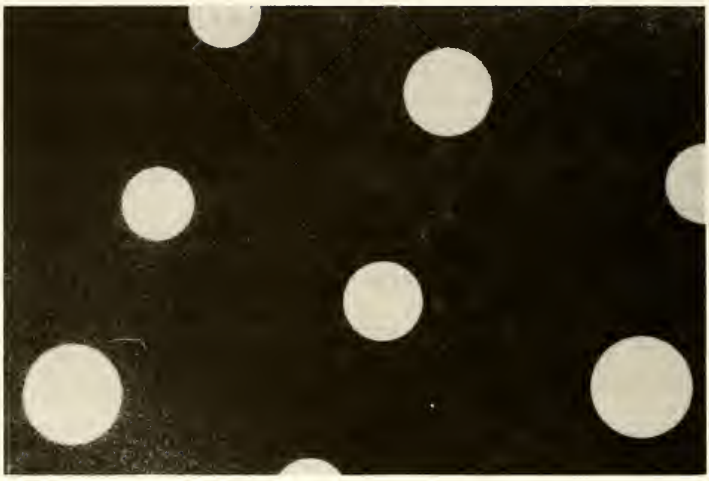

Figure 27

Part of Figure 23

would be necessary to prepare, cut, and measure a special, bulk sample containing spherical particles of a known size distribution to further check the accuracy. However, both figures show that, except the smallest diameter part, the two methods give similar curves of size distributions and that the new method is free of the small-diameter problem that affects the conventional method.

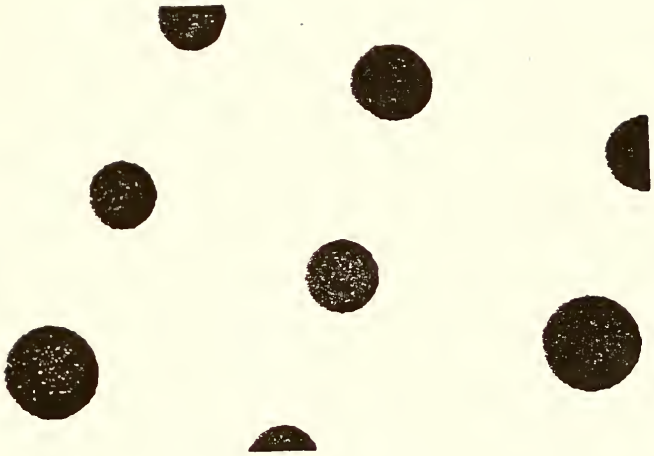

Figure 28

Binary Image of Figure 27

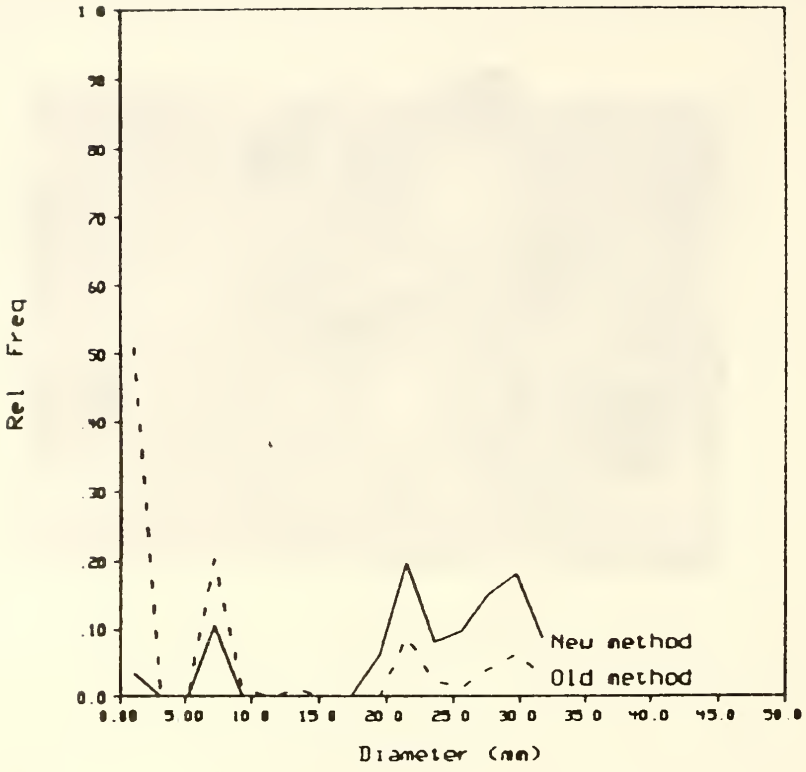

Figure 29

Particle Size Distribution from Fig. 28

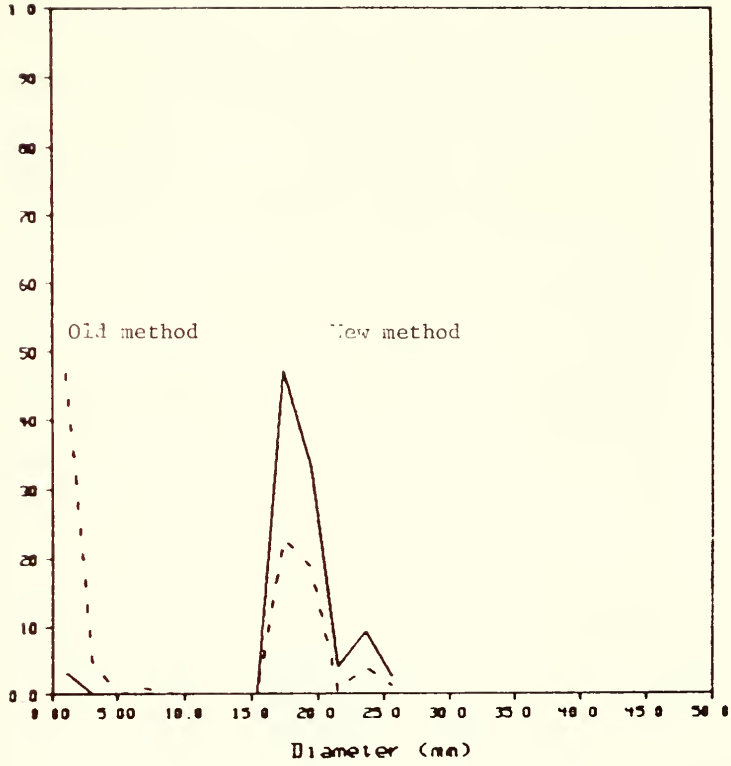

Figure 30

Particle Size Distribution from Fig. 26

GUIDE TO THE USE OF AQIA

The AQIA system is a package of 13 major programs and 6 auxiliary programs. The following flow chart shows the functions and order of use of the 13 major programs.

First, DSCRB initiates the package. It creates a file to hold the processed image. In the file, the initiation time will be recorded automatically. DSCRB also allows the user to briefly describe the sample from which the image has been taken, and to enter the length of one pixel. The binary image and other relevant information will be appended to this file.

REDUCE extracts the image gray level data from the raw image file produced by a digitizer. It also allows the user to reduce the image size and/or the number of gray levels. REDUCE produces a reduced image. After REDUCE, the user must select the method of segmentation.

AQIA has two ways to segment a digital image: straight gray level histogram and edge-detection histogram thresholding. If straight histograming is selected, HISTO will be called next. It compiles a histogram of the

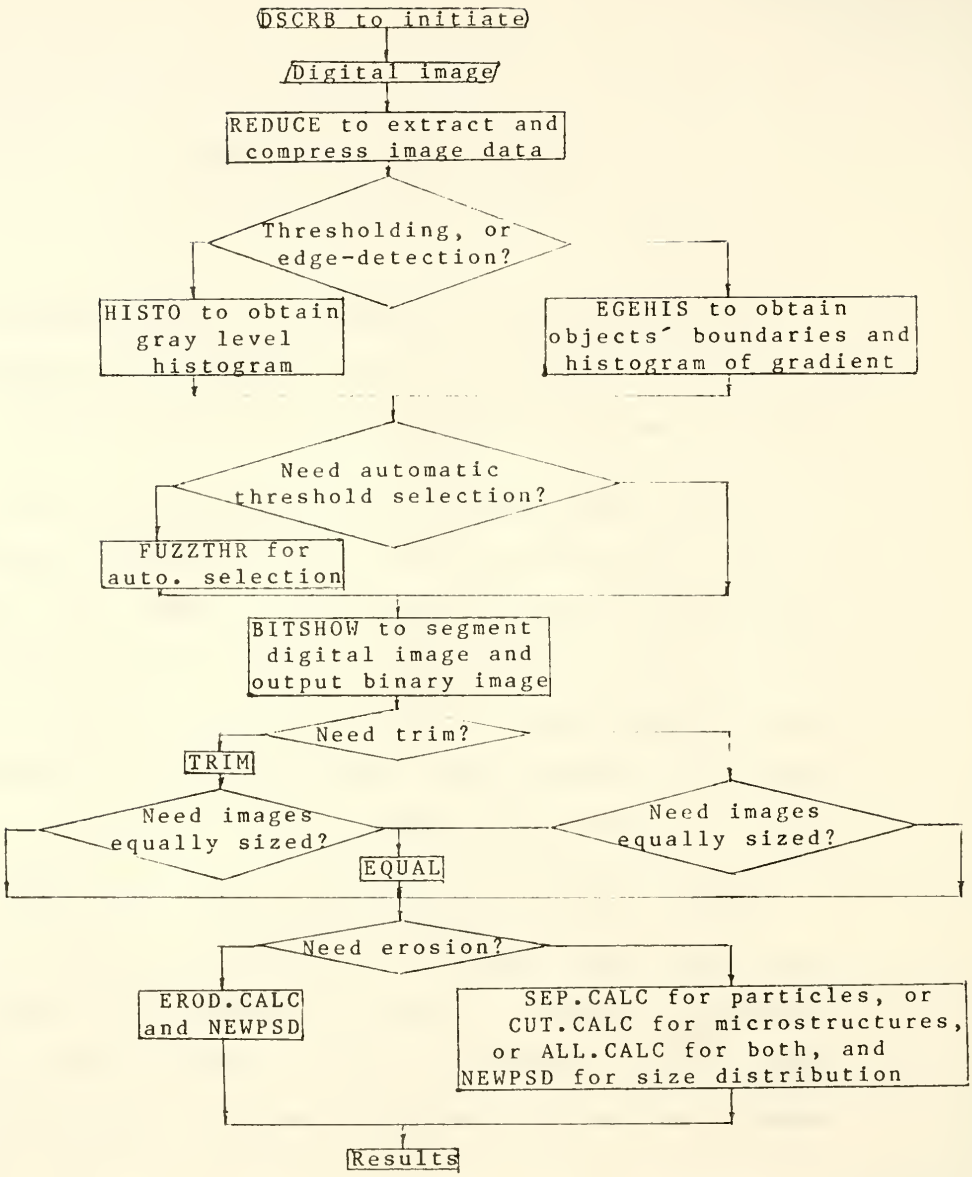

Figure 31

Flow Chart

occurrency of various gray levels. If edge-detection is selected, EGEHIS will be called instead. It singles out

the boundaries of objects, and compiles a histogram of the occurrency of gray level gradients.

Then, the user must decide if he/she wants automatic selection of thresholds from either histogram. If the user chooses the automatic method. FUZZTHR must be called next. FUZZTHR will suggest thresholding bounds.

With or without automatic thresholding, BITSHOW must be called next. BITSHOW asks the user to enter the lower and upper bounds for thresholding. It then displays the binary image on the screen with pixels between the bounds being illuminated. It allows the user to change the bounds until he/she is satisfied with the binary image. If there are some spots in the objects that need to be filled, 'bitshow' allows the user to choose either the overall or individual filling mode, or the individual followed by the overall mode. It outputs the spot-free binary image to the file created by DSCRB.

Next, the user must decide if he/she needs to trim the borders from the binary image. If the user needs this, TRIM will be called next. If there is more than one image of the same sample, the user may call EQUAL to cut these images to the same size, in order to make statistical calculations meaningful.

After this, the user must decide if he/she needs erosion on the binary image before measurement. If erosion is

desired, EROD.CALC will be called next. It allows the user to choose either the overall or individual mode of erosion, or the overall followed by the individual mode. After erosion, the appropriate dilation will be performed. Then, the desired measurements will be performed on the processed binary image. EROD.CALC can perform measurements on projections of separate particles or sections cut through a solid sample. EROD.CALC will output the final results of the measurements, and the eroded/dilated image.

If no erosion is needed, the binary image can be directly measured by the following three programs. SEP.CALC measures the projections of separated particles. CUT.CALC estimates 3-dimensional properties of microstructures from 2-dimensional measurements on cut planes. ALL.CALC does both. NEWPSD can be used to estimate the size distribution of particles by using the new method, after EROD.CALC, or SEP.CALC, or CUT.CALC, or ALL.CALC.

For the user's convenience, AQIA also provides 6 auxiliary programs. These are:

1. DESIGN
2. SHOW
3. INF
4. HARDCP
5. RESULTS
6. PLOTPREP

DESIGN allows the user to find the number of required images for volume fraction estimation, given the image size, the estimated mean value of the area fraction, the

desired estimation accuracy (half-width) and the desired confidence level.

SHOW simply displays a binary image on the screen, but does not allow processing. INF gives the relevant information on an image such as the size of the binary image, the size reduction factor, the number of gray levels, the percentages of 1 and 0 pixels, the thresholding bounds, etc.. HARDCP gives the user a hard copy of the binary image if the user is working on a Tektronix 4014 terminal equipped with a hardcopy unit.

RESULTS either displays the numeric results of the measuring programs on the screen or prints them on a specified printer. PLOTPREP collects the results of measurements from EROD.CALC, or SEP.CALC, or CUT.CALC, or ALL.CALC, to provide input for plotting by UNIX Qplot programs.

For more details on the execution of the programs and naming files, the user should refer to the separate AQIA User Manual.

SAMPLE AND IMAGE PREPARATION TECHNIQUES

The AQIA system can be generally applied to a broad spectrum of construction materials. But, it requires that the sample and image be properly prepared so that the digital image can be segmented into a good binary image that can be measured with the software package. It is impossible to develop a general image and sample preparation technique for various materials. Therefore, different image and sample preparation techniques have to be developed for various materials.

Any photograph can be digitized, processed and measured. A photograph can be taken with an ordinary camera, or through a light microscope, or in an electron microscope. This depends on the magnification that is needed for measuring the objects of interest. The magnification issue will be discussed later.

Either negatives or positives can be digitized. Some digitizers are good for both. Some are only good for one of them. Negatives are recommended if an appropriate digitizer is available, because positives will need additional film processing that will reduce the image quality.

The maximum image size is limited by the memory space of the computer and the resolution of the monitor. In this work, a Tektronix terminal was used as the monitor. It has a 780 x 1024 pixel display area. AQIA allows an image as big as 680 x 1000 pixels. (A 100 pixel high space is left for user-program interaction.) Since AQIA is implemented on the UNIX operating system at Purdue, the memory of the available computers is more than enough for an image of this size. If a digital image is greater than this size, the 'reduce' program can be used to reduce the image size by multiples of two. 'Reduce' also automatically cuts an image's size to 680 x 1000 pixels even if no reduction factor is used. The user must be aware of the monitor display limitation before he/she makes the original image in order that no objects of interest will be cut off by 'reduce'. The bigger the image is, the more computational time it needs. Therefore, it is recommended that the image size be minimized to only include necessary information.

In this work, an ISI Super III-A SEM and an Olympus light microscope were used. Both have a photomicroscopy attachment that uses 35mm film. Although a large format film such as 4'' x 5'' could also be used, it would produce a huge image relative to the resolution of most digitizers. Such an image would need to be reduced. Therefore, 35mm film is recommended.

After the size of the whole image is determined, the resolution that the AQIA will work with has to be chosen. The resolution of the AQIA system is the resolution of the digitizer divided by the magnification of the microscope (if the microscope is used). It is not true that an indefinitely higher resolution necessarily leads to a better image. Too high resolution will often produce spurious objects in the binary image. The user must choose such a resolution that the AQIA system can 'see' the objects of interest and avoid 'seeing' finer objects that are of no interest.

The resolution of a digitizer is the length of one pixel. This information is available from the manufacturer. Sometimes, the resolution is specified as the number of pixels in the orthogonal directions. A simple way to calibrate the lengths of one pixel in these orthogonal directions is to measure the lengths of the sides of the real image and compare them with the numbers of rows and columns of the digital image that are given by the 'reduce' program. Some digitizer do not produce square pixels. The above comparison will indicate if this is the case. The AQIA system assumes that the pixels are square and will give erroneous results if this is not true.

If a light microscope with a photomicroscopy attachment is used, it should be noted that the magnification on the film plane may be different from that on the human's

vision plane. When the user chooses the magnification, it must be the magnification on the film plane.

In summary, the process of obtaining and digitizing a useful image is as follows. First, one decides on the size of the smallest features that is of interest. Then, with a knowledge of the resolution of the digitizer that will be used, one selects a magnification. Finally, one takes a picture of a size that, when digitized at the selected resolution, will be displayable on the monitor.

If a photograph is improperly mounted in a digitizer, the area beyond the image of interest will also be digitized. Although the 'trim' program can remove this area, this wastes file space and processing time. Therefore, the user should be careful when mounting the photograph in the digitizer. Also, the photograph must be parallel to the lens plane of the digitizer to avoid the distortion that will produce pixels with different scales in orthogonal directions.

Segmentation quality heavily depends on the contrast of the original image. The more contrast the original image has, the easier, and more accurate, the segmentation will be. If the image is taken with an ordinary camera, or a light microscope, appropriate lighting and background are needed to strengthen the contrast. If the scanning electron microscope is used, edges and elevated points on

the objects will be brighter. Therefore, a flat surface must be used. The brightness is also affected by the atomic number of the elements present, assuming no coating is used. Therefore, special materials might be used to, for example, fill cracks or voids, to brighten these features.

SEM has another special problem. The scan line moves continuously so that there is no still field of view. Therefore, it is difficult to focus the image. The user must pay more attention and patience to focusing in order to avoid fuzzy images. In SEM, the sample is illuminated only when it is scanned. Therefore, exposure time is fixed, and only the aperture can be changed.

Non-uniform illumination will produce images that are difficult to segment. The images of coins that have been used in this work are an example of non-uniform illumination. This problem can be especially severe in a light microscope at low magnification and extra lighting is needed to increase the uniformity of the illumination.

The current AQIA system only uses gray levels, or their gradients, to differentiate the objects from the background. It can not analyze the texture of a surface. Therefore, if the microstructures in a matrix need to be measured, the sample may need to be polished so that surface texture will not artificially affect the gray levels.

Images that contain pore space such as air voids and cracks can present a special problem if these pores are the objects of interest. The sample must be well polished. However, the digital image may still be difficult to segment. It is suggested that the pores be filled with a contrasting fine powder or a dye, or impregnated with polymers, that will make the pores much lighter or darker than the background. Another approach might be to illuminate the surface at an extremely flat angle so that they would be in deep shadow.

Images of collections of fine particles such as flyash present another problem. The fine particles tend to agglomerate. The ´erod.calc.´ program can´t separate objects that are above one another. And, erosion to separate many particles in the same plane uses considerable computation time. Therefore, fine particles should be separated as much as possible before the image is made. It has been found helpful to disperse such particles in a clear liquid that contains a small amount of a detergent. However, the detergent also introduces air bubbles that may appear in the segmented image. A more effective dispersent may be needed that does not produce air bubbles.

Much of the above advice concerning sample preparation may be summarized as follows. A human viewer of an image brings a broad variety of knowledge to the problem

of segmenting what he/she sees. The AQIA system must depend solely on gray level differences. Thus, the experimenter must keep this in mind, and must arrange for the objects of interest to have a clearly unique gray level that is uniform across the field of view.

CONCLUSIONS

1. An automatic, quantitative image analysis (AQIA) system has been developed for construction materials.

2. A special statistical procedure has been developed that yields the estimation accuracy of a volume fraction analysis for a given number of images of a given size.

3. A special technique of image segmentation, based on the concepts of fuzzy probability, has been developed. It models the cognition process of humans, and produces consistent binary images.

4. The system uses object labeling to process the binary images more accurately and safely than non-labeling image analysis systems.

5. Object labeling makes the processes of object counting and measurement of individual objects as straightforward as the overall measurements.

6. The system can be expected to make measurements with an error of less than 1% with an image of appropriate resolution.

7. In the case of discrete particles, the system can measure the perimeters, areas, maximum chords of the particles, the maximum, minimum and mean values of these parameters, the distributions of these parameters, the area fraction of the particles and the total number of particles.

8. In the case of a cut surface through a massive sample, the system can estimate the volume fraction of objects, the surface area of objects per unit bulk volume, and the surface area of objects per unit object volume. Assuming that the objects are spheres, the particle size distribution of objects in a massive sample, the total number of objects per unit bulk volume and the mean diameter can also be estimated.

9. A computer simulation method has been developed to estimate the size distribution of particles of any modelable shape in a massive sample. This does not have the tendency to artificially inflate the number of small particles as does the conventional procedure.

10. A new software system could be developed to allow the user to assume different shapes for particles in a massive sample and find the most reasonable assumption if the shape of the particles is unknown.

LIST OF REFERENCES

LIST OF REFERENCES

1. Underwood, E.E., Quantitative Stereology, pp. 1-48, Addison-Wesley, Reading, Massachusetts, 1970,

2. Dehoff, R. T., The statistical background of quantitative metallography, Quantitative Microscopy, Dehoff, R. T. and Rhine, F. N. eds., pp. 12-45, McGraw-Hill, New York, 1968,

3. Chatterji, S. and Gudmundsson, H., Characterization of entrained air bubble systems in concretes by means of an image analysing microscope, Cement and Concrete Research, Vol. 7, pp. 423-428, 1977.

4. Gudmundsson, H. et al., The Measurement of paste concrete in hardened concrete using automatic image analyzing technique, Cement and Concrete Research, Vol. 9, pp. 607-612, 1979.

5. Roberts, L. R. and Scali, M. J., Factors affecting image analysis for measurement of air content in hardened concrete, Proceeding of the Sixth International Conference on Cement Microscopy, 1984

6. Roberts, L. R. and Scheiner, P., Microprocessor-based linear traverse apparatus for air-void distribution analysis, Proceeding of the Third International Conference on Cement Microscope, 1982.

7. Kelly, P. M., Quantitative electron microscopy, Metal Forum, Vol. 5, No. 1, 1982, pp. 13-23

8. Oppenheim, J. C., Basic quantitative image analysis in metallographic laboratory, Metal progress, Aug. 1981, pp.36-46

9. Dekaney, A., Particles by the digits, Ind. Res., Jan. 1974, pp. 45-48

10. Lee, R. J., Spitzig, J. F. and Fisher, R. M., Quantitative metallography by computer-controlled scanning electron microscopy, J. Metal, March, 1981, pp. 20-25

11. Davis, D. L. and Lundin, D., Area fraction analysis of multiphase metal systems using a digital segmentation technique, Microstructural Science, Vol. 7, Le May, Fallon and McCall, eds., pp. 433-436, American Slsevier, New York, 1975

12. Rosenfeld, A. and Kak, A. C., Digital Picture Processing, 2nd Ed., pp. 1-9, Academic Press, Orlando, Florida, 1982,

13. Hilliard, J.E., Measurement of volume in volume, Quantitative Microscopy, DeHoff, R. T. and Rhines, F. N. eds., pp. 45-78, McGraw-Hill, New York, 1968,

14. Hilliard, J.E. and Cahn, J.W., An evaluation of procedures in quantitative metallography for volume-fraction analysis, Trans. Met. Soc. of AIME, Vol. 221, 1961, pp. 344-352.

15. Weszka, J. S., A survey of threshold selection techniques, Computer Graphics and Image Processing, Vol. 7, 1978, pp. 259-265

16. Weszka, J. S. and Rosenfeld, A., Threshold evaluation techniques, IEEE Trans. SMC, Vol. SMC-8, No. 8, 1978, pp. 622-629

17. Levy, J. D. and Kelly, T., Development of stereological principles through images analysis and applications to quantitative metallography, Microstructural Science, Vol. 3, French, P. M., Gray, R. J. and McCall, J. L. eds., pp. 387-403, American Elsevier, New York, 1975

18. Hughes, A. and Grawoig, D., Statistics: A foundation for analysis, pp. 162-180, Addison-Wesley, Reading, Massachusetts, 1971

19. Rosenfeld, A. and Kak, A. C., Digital Picture Processing, 2nd Ed., pp. 57-61, Academic Press, Inc., Orlando, Florida, 1982

20. Fugunaga, K., Introduction to Statistical Pattern Recognition, Ch. 3-4, Academic Press, Orlando, Florida, 1972

21. Ahuja, N. and Rosenfeld, A., A note on the use of second-order gray level statistics for threshold selection, IEEE Trans. SMC, Vol. SMC-8, No. 12, 1978, pp. 895-898

22. Deravi, F. and Pal, S. K., Gray level thresholding using second-order statistics, Pattern Recognition Letters, Vol. 1, 1983, pp. 417-422

23. Rosenfeld, A. and Torre, P. D., Histogram concavity analysis as an aid in threshold selection, IEEE Trans. SMC, Vol. SMC-13, No. 3, 1983, pp. 231-235

24. Otsu, N., A threshold selection method from gray level histogram, IEEE Trans. SMC., Vol. SMC-9, No. 1, 1979, pp. 62-66

25. Weszka, J. S. and Rosenfeld, A., Histogram modification for threshold selection, IEEE Trans. SMC, Vol. SMC-9, No. 1, 1979, pp. 38-52

26. Kirby, R. L. and Rosenfeld, A., A note on the use of (gray level, local average gray level) space as an aid in threshold selection, IEEE Trans. MSC, Vol. SMC-9, No. 12, 1979, pp. 860-868

27. Chanda, B., Chaudhuri, B. B. and Majumder, D. D., On image enhancement and threshold selection using the graylevel co-occurence matrix, Pattern Recognition Letters, Vol. 3, 1985, pp. 243-251

28. Gupta, M. M., Computer vision with the fuzzy algorithms, presented at the Workshop of NAFIPS, Purdue University, W. Laf. Indiana, May 5-7, 1987

29. Pal, S. K. and R. A. King, Image enhancement using fuzzy set, Electronic Letters, Vol. 16, No. 10, 1980, pp 376-378

30. Pal, S. K. and R. A. King, Image enhancement using smoothing with fuzzy set, IEEE Trans. SMC, Vol. SMC -11, No. 7, 1981, pp 494-501

31. Pal, S. K. and R. A. King, Automatic gray level thresholding through index of fuzzyness and entropy, Pattern Recognition Letters, Vol. 1, 1983, pp 141-146

32. Pal, S. K., Fuzzy set theoretic approach: a tool for speech and image recognition, Pattern Recognition Theory and Applications, Kittler, J., Fu, K. S. and Pau, L. F. eds., pp. 103-117,

33. Zadeh, L. A., Probability measure of fuzzy events, J. Math. Anal. and Appl., Vol. 23, 1968, pp 421-427

34. Satty, T. L., Measuring the fuzziness of sets, J. Cybernetics 4, 1974, pp 53-61

35. Santamarina, J. C. and Chameau, J. L., From crispness to fuzziness: A simplified method to construct membership functions, to be published by Fuzzy Sets and Systems

36. Leitz TAS Reference Manual, Ernst Leitz Wetzlar GmbH and Bosch Fernseh- Anlagen GmbH, W. Germany

37. Russ, J. C., Image processing in a general purpose microcomputer, J. Microscopy, Vol. 135, Pt 1, July 1984, pp.89-102

38. Rosenfeld, A. and Kak, A. C., Digital Picture Processing, 2nd Ed., pp. 240-244, Academic Press, Inc., Orlando, Florida, 1982.

39. Hunn, W., New techniques in image analysis as applied to the metallographic specimen, Microstructural Science, Vol. 3, French, P. M., Gray, R. J. and McCall, J. L. eds. pp. 375-387, American Elsevier, New York, 1975

40. Bradbury, S., Microscopical image analysis: problems and approaches, J. Microscopy, Vol. 115, Pt. 2, 1979, pp.137-150

41. Underwood, E. E., Surface area and length in volume, Quantitative Microscopy, DeHoff, R. T. and Rhines, F. N., eds. pp. 78-128, McGraw-Hill, New York, 1968

42. Underwood, E. E., Particle size distribution, Quantitative Microscopy, DeHoff, R. T. and Rhines, F. N., eds. pp. 151-200, McGraw-Hill, New York, 1968

43. Hughes, A. and Grawoig, D., Statistics: A foundation for analysis, pp. 21-35, Addison-Wesley, Reading, Massachusetts, 1971

44. Coleman, R., Random paths through rectangles and cubes, Metallography, Vol. 6, 1973, pp. 103-114

45. Exner, H. E. and Lukas, H. L., The experimental verification of the stationary Wagner-lifshitz distribution of coarse particles, Metallography, Vol. 4, 1971, pp. 325-338

46. Warren, R. and Naumovich, N., Relative frequencies of random intercepts through convex bodies, J. Micros. Vol. 110, Pt. 2, 1977, pp. 113-120

Appendix A

Basic Statistical Equations

This appendix will give some basic statistical equations used in the thesis and the appendices.

1. If x is a discrete random variable, the mean of k x's is:

$$\bar{x} = \sum_{i}^{k} x_i \, p(x_i) \tag{A.1}$$

where $p(x_i)$ is the probability function.

The variance with respect to $\bar{x}$ is:

$$\begin{aligned} \sigma^2(x) &= \sum_{i}^{k} (x_i - \bar{x}) p(x_i) \\ &= \sum_{i}^{k} x_i^2 p(x_i) - \bar{x}^2 \end{aligned} \tag{A.2}$$

or

$$\sigma^2(x) + \bar{x}^2 = \sum_{i}^{k} x_i^2 p(x_i) \tag{A.3}$$

The variance with respect to some constant c is:

$$\begin{aligned} \sigma^2(x)_c &= \sum_{i}^{k} (x_i - c)^2 p(x_i) \\ &= \sigma^2(x) + (\bar{x} - c)^2 \end{aligned} \tag{A.4}$$

2. If y is a linear function of x as:

$$y = \sum_{i}^{k} c_i \, x_i$$

the variance of y is:

$$\sigma^2(y) = \sum_i^k c_i{}^2 \sigma^2(x_i) \qquad (A.5)$$

where c_i's are constants.

3. Given event y, the probability that the event x occurs is $p(x|y)$. So the probability that x accurs is:

$$p(x) = p(x|y)\ p(y) \qquad (A.6)$$

If x also occurs when event z occurs, the total probability that x occurs is:

$$p(x) = p(x|y)\ p(y) + p(x|z)\ p(z) \qquad (A.7)$$

In general,

$$p(x) = \Sigma\ p(x|y_i)\ p(y_i) \qquad (A.8)$$

This means that x occurs when any y_i occurs.

Appendix B

Coefficient of Variation of Area Fractions

Suppose there are n sections (planes cut through the material), each with the same area A, and an area fraction of features $(A_A)_j$ (j = 1,2,.....n). On each section, the cross sectional areas of intercepted features are grouped into k classes of size a_i (i = 1,2,.....k). $(m_i)_j$ is the number of intercepted features with cross area a_i on section j. The area fraction on section j is the average over k classes, with class i having m_i intercepted features of cross area a_i:

$$(A_A)_j = \sum_i^k (m_i)_j \frac{a_i}{A} \qquad (B.1)$$

The mean area fraction from n sections is the average over n area fraction measurements:

$$\begin{aligned} \overline{A_A} &= \frac{\sum_j^n (A_A)_j}{n} \qquad (B.2) \\ &= \frac{1}{nA} \sum_j^n \sum_i^k (m_i)_j \, a_i \\ &= \frac{1}{nA} \sum_i^k a_i \sum_j^n (m_i)_j \\ &= \frac{1}{A} \sum_i^k a_i \sum_j^n \frac{(m_i)_j}{n} \\ &= \frac{1}{A} \sum_i^k a_i \, \overline{m_i} \end{aligned}$$

Since the features are assumed to be randomly distributed in the matrix, m_i is a random variable that is the number of intercepted features with cross area a_i appearing within a given area A. m_i will follow a Poisson distribution. For Poisson distributions, the variance and the mean of the random variable are equal to each other, as:

$$\sigma^2(m_i) = \overline{m_i} \tag{B.3}$$

The following applies to each section, therefore the subscript j can be omitted and Eqn. B.1 can be written as:

$$A_A = \sum_i^k m_i \frac{a_i}{A} \tag{B.4}$$

Applying Eqn. A.5 results in:

$$\sigma^2(A_A) = \frac{1}{A^2} \sum_i^k a_i^2 \, \sigma^2(m_i) \tag{B.5a}$$

or, in view of Eqn, B.3:

$$\sigma^2(A_A) = \frac{1}{A^2} \sum_i^k a_i^2 \, \overline{m_i} \tag{B.5b}$$

Deviding (B.5b) through by $\overline{M_a}$ gives:

$$\frac{\sigma^2(A_A)}{\overline{M_a}} = \frac{1}{A^2} \sum_i^k a_i^2 \, \frac{\overline{m_i}}{\overline{M_a}} \tag{B.6a}$$

If $p(a_i)$ is defined as the probability that a intercepted feature with cross area a_i is observed within the total $\overline{M_a}$ intercepted features, then

$$p(a_i) = \frac{\overline{m_i}}{\overline{M_a}}$$

and

$$\frac{\sigma^2(A_A)}{\overline{M}_a} = \frac{1}{A^2} \sum_i^k a_i^2 \, p(a_i) \qquad (B.6b)$$

Since Eqn. A.3 may be written in the present nomenclature as:

$$\sigma^2(a) + \overline{a}^2 = \sum_i^k a_i^2 \, p(a_i) \qquad (B.7)$$

Eqn. B.6b becomes:

$$\frac{\sigma^2(A_A)}{\overline{M}_a} = \frac{1}{A^2} (\sigma^2(a) + \overline{a}^2) \qquad (B.8)$$

Squaring Eqn. B.2 and then deviding it through by $\overline{M}_a^2$ gives:

$$\frac{\overline{A}_A^2}{\overline{M}_a^2} = \frac{1}{A^2} \left| \sum_i^k a_i \frac{\overline{m}_i}{\overline{M}_a} \right|^2 \qquad (B.9)$$

$$= \frac{1}{A^2} \left| \sum_i^k a_i \, p(a_i) \right|^2$$

Since Eqn. A.1 may be written in the present nomenclature as:

$$\overline{a} = \Sigma \, a_i \, p(a_i) \qquad (B.10)$$

Eqn. B.9 becomes:

$$\frac{\overline{A}_A^2}{\overline{M}_a^2} = \frac{\overline{a}^2}{A^2} \qquad (B.11)$$

Combining Eqn. B.8 and B.11 gives Equation 1 in the main

Appendix C

Coefficient of Variation of Cross-sectional Areas

The value of $\sigma^2(a)/\bar{a}^{-2}$ depends on the shape of the intercepted feature. The simplest case is a sphere with diameter 2r. The following figure shows a circular disc formed by the intersection of the sphere with a plane of thickness dh. The disc has a radius r cos(θ), where θ indicates the orientation of the disc.

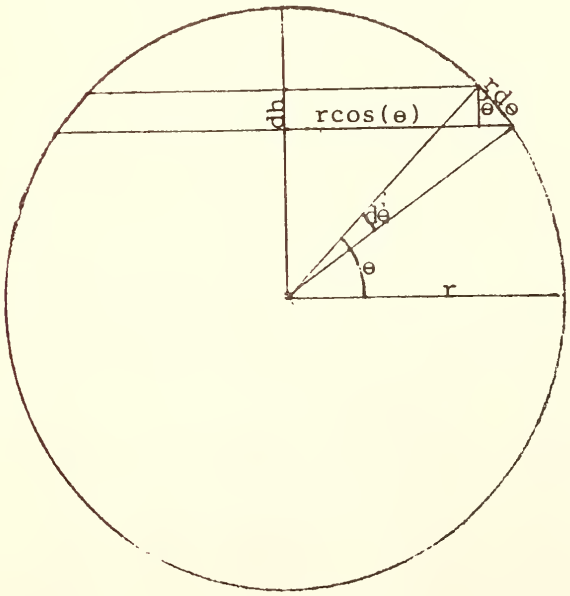

The area of the disc, a_θ, is:

$$a_\theta = \pi r^2 \cos^2(\theta),$$

The thickness of the disc, dh, is:

$$dh = (r\ d\theta)\ [\cos(\theta)]$$

The probability that a disc with oreintation θ occurs is:

$$\frac{dh}{r} \text{ or } \frac{2\ dh}{2\ r},$$

this is:

$$\frac{r d\theta\ \cos(\theta)}{r}$$

Applying Eqn. A.1 results in the mean cross sectional area as:

$$\bar{a} = \int_0^{\frac{\pi}{2}} (\pi r^2 \cos^2\theta) \frac{r d\theta\ \cos\theta}{r} \qquad (C.1)$$

$$= \pi r^2 \int_0^{\frac{\pi}{2}} \cos^3\theta\ d\theta$$

$$= \frac{2}{3}\pi r^2$$

Applying Eqn. A.2 results in the variance of the cross sectional areas as:

$$\sigma^2(a) = \int_0^{\frac{\pi}{2}} (\pi r^2 \cos^2\theta)^2 \frac{r d\theta\ \cos\theta}{r} - \bar{a}^2 \qquad (C.2)$$

$$= \frac{4}{45}\pi^2 r^4$$

Dividing Eqn. C.2 by the square of $\bar{a}$ gives:

$$\frac{\sigma^2(a)}{\bar{a}^2} = 0.2 \qquad (C.3)$$

For a less regular shape, a bigger value is expected [2].

Appendix D

100(1 - α/2) Percentile of t Distribution

Table 16

100(1 - α/2) Percentile of t Distribution [43]

Sample Size - 1	Conf. Level	
	0.95	0.90
1	12.706	6.314
2	4.303	2.920
3	3.182	2.353
4	2.776	2.132
5	2.571	2.015
6	2.447	1.943
7	2.365	1.895
8	2.306	1.860
9	2.262	1.833
10	2.228	1.812
11	2.201	1.796
12	2.179	1.786
13	2.160	1.771
14	2.145	1.761
15	2.131	1.753
16	2.120	1.746
17	2.110	1.740
18	2.101	1.734
19	2.093	1.729
20	2.086	1.725
21	2.080	1.721
22	2.074	1.717
23	2.069	1.714
24	2.064	1.711
25	2.060	1.708
26	2.056	1.706
27	2.052	1.703
28	2.048	1.701
29	2.045	1.699
30	2.042	1.697
>30	2.000	1.671

Appendix E

Questionaire for Darkness Pair by Pair Comparison

Table 17

Questionaire for Darkness Pair by Pair Comparison

Observer's Assessment	Number Equivalent
The squares are the same.	1
One square is very slightly darker than the other.	2
One square is slightly darker than the other.	3
One square is somewhat darker than the other.	4
One square is considerably darker than the other.	5
One square is much darker than the other.	6
One square is very much darker than the other.	7

One black square and one white were considered as the extremes. By definition, the black square was rated as "very much darker than" the white one.

COVER DESIGN BY ALDO GIORGINI